



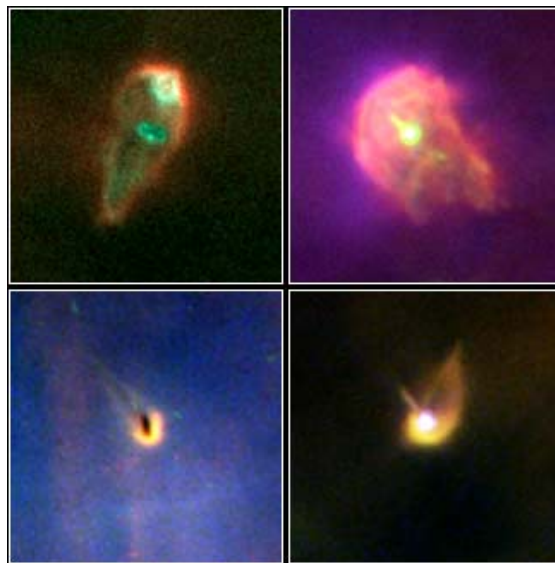
UNIVERSITY OF GRONINGEN

KAPTEYN ASTRONOMICAL INSTITUTE

Spectral Energy Distributions of Protoplanetary Disks in the Orion Nebula

Author:
Walter VAN ROSSEM

Supervisor:
Silvia VICENTE



June 2014

Abstract

Proplyds are young stellar objects which are typically teardrop shaped with a head and a tail because they are being heated and ionized by nearby OB stars. In this work various photometric catalogues are compiled and searched for these proplyds using scripts that were written for this purpose. Presented are the spectral energy distributions of known proplyds in the Orion Nebula ranging from the optical to the submillimeter. Further steps for this work include adding the X-ray and far infrared regimes to the spectral energy distributions, as well as comparing these spectral energy distributions to models of proplyds to find some of their properties.

The coverpage image shows four proplyds in the Orion Nebula using the *Hubble Space Telescope* WFPC2 instrument in filters [NII] (red), H α (green), and [OIII] (blue). Image credit: NASA, ESA, J. Bally, H. Throop, and C. R. O'Dell

Contents

1	Introduction	5
2	Data	7
2.1	Photometric Catalogues	7
2.2	Extinction Catalogues	10
2.3	Data Products	10
3	Spectral Energy Distributions	14
3.1	Scripts	14
3.1.1	Importing and extracting data	14
3.1.2	Cross-identification and correcting for astrometric shifts	16
3.1.3	Astrometric shift in catalogue tables	17
3.1.4	Manipulating Data	19
3.2	SEDs	22
3.2.1	Ionized objects	24
3.2.1.1	No star or disk visible inside cocoon	24
3.2.1.2	Only star visible inside cocoon	26
3.2.1.3	Star and disk visible inside cocoon	28
3.2.1.4	Only disk visible inside cocoon	30
3.2.2	Pure silhouettes	32
3.2.3	Reflection Nebulae	34
3.2.4	Jets	36
4	Variability	38
4.1	Script	38
4.2	Variability Plots	39
5	Analysis and Discussion	43
6	Conclusion	47
7	Acknowledgments	48
8	Bibliography	48

1 Introduction

The Orion Nebula (M42) is the nearest young high mass star forming region ($d \approx 414 \pm 7$ pc) (Menten et al. 2007). This makes it an excellent location in which we can study star and planet formation as it contains stars with masses ranging down to a few Jupiter masses (Muench et al. 2002) and up to 38 solar masses (Kraus et al. 2009). We think the Sun formed in the neighborhood of high mass stars as there are indications of a recent nearby supernova (Boss et al. 2008). Hence the Orion Nebula is often called the prototype region to study star and planet formation similar to our own. In 1979 a few compact ionized sources were discovered using [OIII], $H\alpha$, and [NII] narrow-band filters at the *Pic-du-Midi* Observatory (Laques & Vidal 1979). They were subsequently also observed using the *Very Large Array* (VLA) in 1987 (Garay et al. 1987). Ever since then the Orion Nebula has been a region of interest for astronomers. Since the 1990s the *Hubble Space Telescope* (HST) has been used to observe these objects and has greatly helped in uncovering their nature. In 1993 the HST was used to observe the central region of the Orion Nebula, and found these objects to be externally ionized PROtoPLANetary Disks (proplyds) (O’Dell et al. 1993). Proplyds are a class of Young Stellar Objects (YSOs) usually found within a cocoon of ionized hydrogen. They are YSOs due to a variety of reasons. First of all, they still have a disk around their star. The disk is formed by the conservation of angular momentum of the protostar during its collapse. Other reasons are that their position in the Hertzsprung–Russell diagram, the fact they are part of the Orion Nebula, and their spectral types and models all suggest that they are young objects as well. The structure of a typical proplyd in Orion can be seen in figure 1. The disk is heated by far-ultraviolet (FUV) from OB stars which penetrates deeper than the extreme-ultraviolet (EUV). This heating creates a high temperature and high density region. The material in this region will expand and flow out of the disk. This outflow is much less dense than the disk and so can be ionized by EUV radiation from nearby OB stars in the Trapezium. This scenario has been described by both analytical and numerical models (Johnstone et al. 1998; Störzer & Hollenbach 1999; Richling & Yorke 2000). The proplyds are typically tadpole-shaped with a head and a tail. The head of a proplyd usually has a bright photoionization front pointing towards the source of ultraviolet radiation, and the tail points in the direction of the local flow. These tails are thought to be produced by diffuse FUV radiation. The size of the visible disks of the proplyds in the Orion Nebula are typically 100-200 AU (Vicente & Alves 2005). In our Solar System, the remnants of this disk are thought to be located in the Kuiper belt (Luu & Jewitt 2002). The Kuiper belt stretches from roughly 30 to 55AU, which is well within the observed sizes of disks in the Orion Nebula.

The goal of this project is to create the spectral energy distribution (SED) for the proplyds in the Orion Nebula ranging from the optical to sub-millimeter. The source catalogue on which this work was based originates from the most recent

¹Image credit: William Henney

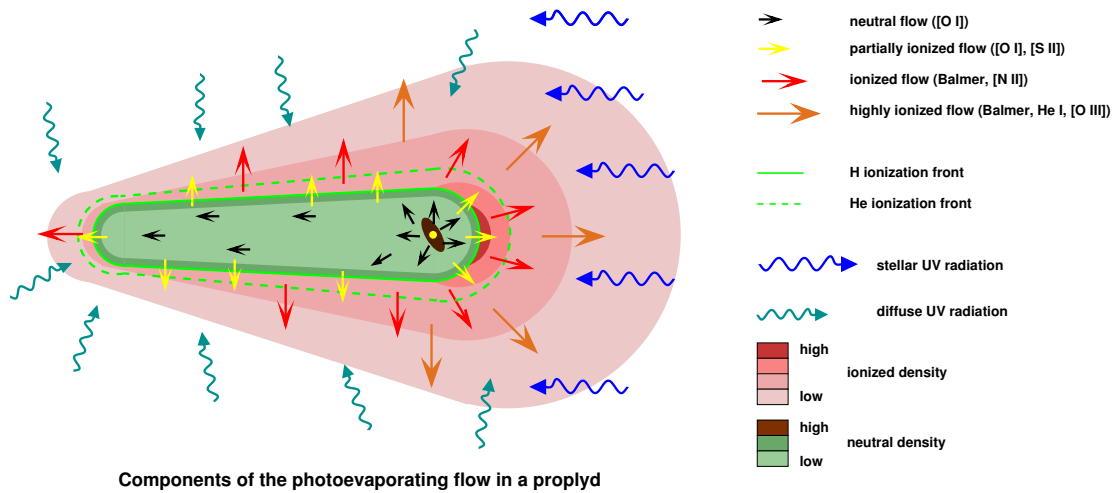


Figure 1: Structure of a typical proplyd. ¹

large *HST* survey of the Orion Nebula, *The HST Treasury Program* by Robberto et al. (2013). The source catalogue is published in the paper by Ricci et al. (2008), *The Hubble Space Telescope Advanced Camera for Surveys Atlas of Protoplanetary Disks in the Great Orion Nebula*. These SEDs are an important part of furthering understand the evolution of protoplanetary disks evolving in a similar environment to where the Sun formed. In dark clouds without bright OB stars, such as those in Taurus or Auriga, the shape of the SEDs can indicate the evolutionary stage of the star and its disk, and modeling allows for physical disk properties to be inferred. Comparing the SEDs of proplyds with those from dark clouds allows us to assess the effect of the external irradiation on the evolution of the protoplanetary disks.

2 Data

This work makes use of various photometric catalogues available in the literature in order to obtain the photometric data for the proplyds. The coordinates of the proplyds used are contained in *The Hubble Space Telescope/Advanced Camera for Surveys Atlas of Protoplanetary disks in the Great Orion Nebula* by Ricci et al. (2008). This paper also provides images of the proplyds in each ACS filter. The photometric catalogues are then searched for sources which are within 2 arcseconds of proplyds in the atlas. If more than one source is found, the nearest source is selected. The photometric data is then extracted from each catalogue and converted from magnitudes to energy density (λF_λ) with units of $\text{erg s}^{-1}\text{cm}^{-2}$. This energy density is then plotted as a function of the wavelength of the associated measurement, in micrometers, to create an SED for each proplyd. In this paper the SEDs range from the optical to the submillimeter, but X-ray surveys do exist for the Orion Nebula. The *Chandra Orion Ultradeep Project (COUP)* is a 838ks survey of the Orion Nebula which captures X-ray sources with energies greater than 0.5keV and is described in Getman et al. (2005b,a). These will be included in the follow up work of the present study. In this work, when describing photometric data “object” refers to sources taken from a given photometric catalogue, while “proplyd” refers to objects taken from the atlas by Ricci et al. (2008).

In order to compare the different photometric points from different instruments and filters they must be converted to energy densities. In order to do this a zero point flux is required. The process in which this is done is described in more detail in section 3.1.4. Where possible this zero point flux is retrieved from the instrument website or from the *Spanish Virtual Observatory Filter Profile Service*. If this is not possible a generic filter specific zero point flux is used. When the photometric point is plotted the ‘Various’ marker and label is used for those points.

2.1 Photometric Catalogues

The data of the following catalogues, except for those by Mann et al. (2014) and Mann & Williams (2010), were obtained from the *VizieR* catalogue access tool, CDS, Strasbourg, France. Those by Mann et al. (2014) and Mann & Williams (2010) were extracted from their respective papers. Two additional photometric points at $8.6\mu\text{m}$ and $11.3\mu\text{m}$ and a spectrum at $11\mu\text{m}$ for the proplyd 182-413 (also known as HST10) were provided by Silvia Vicente and are described in Vicente et al. (2013).

The catalogue by Cutri & et al. (2012) is the *WISE All-Sky Data Release*. The telescope used was the 0.4m *Wide-field Infrared Survey Explorer (WISE)*. This catalogue provides photometry for the W1, W2, W3, and W4 filters with central wavelengths at $3.4\mu\text{m}$, $4.6\mu\text{m}$, $12\mu\text{m}$, and $22\mu\text{m}$ respectively. It also includes *2MASS* (2 Micron All-Sky Survey) photometry for the J ($1.25\mu\text{m}$), H ($1.65\mu\text{m}$), and Ks ($2.17\mu\text{m}$) filters obtained with two identical 1.3m telescopes at the Whipple Observatory and at the Cerro Tololo Inter-American Observatory.

The catalogue by Robberto et al. (2010) is the *Wide-field survey of the Orion*

Nebula Cluster in the Near-Infrared. The telescope used was Cerro Tololo Inter-American Observatory's (CTIO) 4m Blanco telescope and provides photometry for the J, H, and Ks bands. This is the only catalogue that contains both aperture photometry and point spread function (PSF) photometry. The table in the accompanying paper in which the data is contained is table 5.

The catalogue by Kryukova et al. (2012) is the *Luminosity Functions of Spitzer-identified Protostars in Nine Nearby Molecular Clouds*. The telescope used was the 0.85 m *Spitzer Space Telescope*. It contains photometry in the IRAC3.6, IRAC4.5, IRAC5.8, IRAC8.0, and MIPS24 filters. The central wavelengths of these filters are $3.6\mu\text{m}$, $4.5\mu\text{m}$, $5.8\mu\text{m}$, $8.0\mu\text{m}$, and $24\mu\text{m}$, respectively. It also includes J, H, and Ks photometry from *2MASS*. The table in the accompanying paper in which the data is contained is table 1.

The catalogue by Da Rio et al. (2009) is titled *A Multi-color Optical Survey of the Orion Nebula Cluster. I. The Catalog*. The observations were made with the WFI imager at the ESO/MPI 2.2m telescope at La Silla Observatory. It contains photometry for the U, B, V, TiO, and I bands. These filters have central wavelengths at $0.35\mu\text{m}$, $0.45\mu\text{m}$, $0.54\mu\text{m}$, $0.62\mu\text{m}$, and $0.86\mu\text{m}$, respectively. The table in the accompanying paper in which the data is contained is table 2.

The catalogue by Robberto et al. (2013) is *The Hubble Space Telescope Treasury Program on the Orion Nebula Cluster*. It used the Advanced Camera for Surveys (ACS), the Wide-Field Planetary Camera 2 (WFPC2), and the Near-Infrared Camera and Multi-Object Spectrograph (NICMOS) instruments on the *HST*. It contains photometry for 11 filters. The filters used by ACS were F435W, F555W, F658N, F775W, and F850LP. The filters used by WFPC2 were F336W, F439W, F656N, and F814W. Finally, the filters used by NICMOS were F110W, and F160W. The name of the filters for the ACS and WFPC2 instruments indicate the central wavelength in nanometers. For NICMOS the numbers indicate the central wavelength in tens of nanometers. The W, N, or LP at the end of the filter name indicate whether the filter is a Wide-band (W), Narrow-band (N), or a Long-Pass (LP) filter. The paper accompanying this catalogue also provided a mosaic of the Orion Nebula in the averaged F775W and F850LP filters². The tables in the accompanying paper in which the data is contained are tables 5 (ACS), 6 (WFPC2), and 7 (NICMOS).

The catalogue by Lucas et al. (2005), titled *A deep survey of brown dwarfs in Orion with Gemini*, used the 8.1m *Gemini South* telescope at Mauna Kea. It contains photometry for the J, H, and K bands. The table in the accompanying paper in which the data is contained is table 2.

The catalogue by Robberto et al. (2005) is *The Orion Nebula in the Mid-Infrared*. It contains photometry for the N and Q bands with central wavelengths of $10.5\mu\text{m}$ and $20.5\mu\text{m}$ respectively. The table in the accompanying paper in which the data is contained is table 3.

The catalogue by Getman et al. (2005a) is titled *Membership of the Orion Nebula Population from the Chandra Orion Ultradeep Project*. It also contains photometry from Getman et al. (2005b), but also for the V and I bands, as well

²Available at <http://archive.stsci.edu/prepds/orion/>

as *2MASS* J, H, Ks. The table in the accompanying paper in which the data is contained is table 4.

The catalogue by Getman et al. (2005b) is the *Chandra Orion Ultradeep Project: Observations and Source Lists*. It contains a soft X-ray band (0.5-2.0keV) and a hard X-ray band (2.0-8.0 keV). It also contains photometry for the V, I, J, H, Ks, L ($3.5\mu\text{m}$), and *2MASS* J, H, Ks. The tables in the accompanying paper in which the data is contained are tables 9 (V, I), and 10 (J, H, K, L).

The catalogue by Hillenbrand et al. (1998) is titled *Circumstellar Disks in the Orion Nebula Cluster*. It contains photometry in the J, H, K, L ($3.8\mu\text{m}$), M ($4.7\mu\text{m}$), N, and Q bands. The table in the accompanying paper in which the data is contained is table 1.

The catalogue by Feigelson et al. (2002) is titled *X-Ray-emitting Young Stars in the Orion Nebula*. The X-ray photometry presented in this paper is the same as Getman et al. (2005b). However, it contains photometry for the V and H bands. The tables in the accompanying paper in which the data is contained are tables 5 (V), and 6 (H).

The catalogue by Lada et al. (2004) is titled *Deep 3.8 Micron Observations of the Trapezium Cluster*. It contains photometry for the L' band ($3.8\mu\text{m}$) using the 8.2m *Very Large Telescope Unit Telescope 3 (VLT UT3)* at Paranal. The table in the accompanying paper in which the data is contained is table 2.

The catalogue by Hillenbrand & Carpenter (2000) is titled *Constraints on the Stellar/Substellar Mass Function in the Inner Orion Nebula Cluster*. It contains photometry for H and K bands using the 10m *Keck* telescope. The table in the accompanying paper in which the data is contained is table 1.

The catalogue by Hillenbrand (1997) is titled *On the Stellar Population and Star-Forming History of the Orion Nebula Cluster*. It contains photometry for the V and I bands, which originate from different surveys using different telescopes as mentioned in her paper. The table in the accompanying paper in which the data is contained is table 1.

The catalogue by Smith et al. (2005) is titled *Thermal Dust Emission from Proplyds, Unresolved Disks, and Shocks in the Orion Nebula*. It contains photometry for the wide-band Si-5 ($11.6\mu\text{m}$) using the 8m Gemini South telescope. The table in the accompanying paper in which the data is contained is table 1.

The paper by Mann et al. (2014) titled *ALMA Observations of the Orion Proplyds* used the *Atacama Large Millimeter Array (ALMA)* to observe the Orion Nebula at $856\mu\text{m}$. This paper does not have machine readable tables available, and hence the data has to be extracted from the paper. The table in the paper in which the data is contained is table 2.

The paper by Mann & Williams (2010) titled *A Submillimeter Array Survey of Protoplanetary Disks in the Orion Nebula Cluster* used the *SubMillimeter Array (SMA)* to observe the Orion Nebula between $850\mu\text{m}$ and $880\mu\text{m}$. It also contains data for 5 objects at $1330\mu\text{m}$. This paper also does not have machine readable tables available, and hence the data had to be extracted from the paper. The tables in the paper in which the data is contained are tables 2 and 3 (for $850\text{-}880\mu\text{m}$) and table 4 for the $1330\mu\text{m}$ fluxes.

2.2 Extinction Catalogues

There are 3 catalogues that list V-band extinctions: Da Rio et al. (2012), Da Rio et al. (2010), and Hillenbrand (1997). If an object had an entry in multiple catalogues, the extinction was selected from the catalogues in the following order: Da Rio et al. (2012), Da Rio et al. (2010), and then Hillenbrand (1997). If no extinction was available, the median value of 1.5 magnitudes was used. This is the median extinction of objects in the Orion Nebula found by Da Rio et al. (2010). They also shows that using the Cardelli Extinction Law Cardelli et al. (1989) with a reddening parameter $R_V = 3.1$ is more compatible for the Orion Nebula than $R_V = 5.5$ suggested by Costero & Peimbert (1970) as it gave them less negative extinctions during their derivation of extinctions.

2.3 Data Products

Accompanying this work in electronic format are tables containing the flux densities (F_λ) in $\text{erg s}^{-1}\text{cm}^{-2}\mu\text{m}^{-1}$ for each proplyd. The optical to infrared table columns are described in table 1, and the submillimeter table columns are described in table 2. The errors are given in separate tables with the same columns.

Table 1: Description of the columns in the optical to infrared photometry table

Column Index	Source Catalogue	Instrument	Filter	Comments
0	Cutri & et al. (2012)	WISE	W1	
1	Cutri & et al. (2012)	WISE	W2	
2	Cutri & et al. (2012)	WISE	W3	
3	Cutri & et al. (2012)	WISE	W4	
4	Cutri & et al. (2012)	2MASS	J	
5	Cutri & et al. (2012)	2MASS	H	
6	Cutri & et al. (2012)	2MASS	Ks	
7	Robberto et al. (2010)	CTIO/ISPI	J	PSF
8	Robberto et al. (2010)	CTIO/ISPI	H	PSF
9	Robberto et al. (2010)	CTIO/ISPI	Ks	PSF
10	Robberto et al. (2010)	CTIO/ISPI	J	Aperture
11	Robberto et al. (2010)	CTIO/ISPI	H	Aperture
12	Robberto et al. (2010)	CTIO/ISPI	Ks	Aperture
13	Kryukova et al. (2012)	2MASS	J	
14	Kryukova et al. (2012)	2MASS	H	
15	Kryukova et al. (2012)	2MASS	Ks	
16	Kryukova et al. (2012)	Spitzer	IRAC3.6	
17	Kryukova et al. (2012)	Spitzer	IRAC4.5	
18	Kryukova et al. (2012)	Spitzer	IRAC5.8	
19	Kryukova et al. (2012)	Spitzer	IRAC8.0	
20	Kryukova et al. (2012)	Spitzer	MIPS24	
21	Da Rio et al. (2009)	WFI	U	
22	Da Rio et al. (2009)	WFI	B	
23	Da Rio et al. (2009)	WFI	V	
24	Da Rio et al. (2009)	WFI	TiO	
25	Da Rio et al. (2009)	WFI	I	
26	Robberto et al. (2013)	HST ACS	F435W	Undrizzled
27	Robberto et al. (2013)	HST ACS	F555W	Undrizzled
28	Robberto et al. (2013)	HST ACS	F658N	Undrizzled
29	Robberto et al. (2013)	HST ACS	F775W	Undrizzled
30	Robberto et al. (2013)	HST ACS	F850LP	Undrizzled
31	Robberto et al. (2013)	HST ACS	F435W	Drizzled
32	Robberto et al. (2013)	HST ACS	F555W	Drizzled
33	Robberto et al. (2013)	HST ACS	F658N	Drizzled
34	Robberto et al. (2013)	HST ACS	F775W	Drizzled
35	Robberto et al. (2013)	HST ACS	F850LP	Drizzled
36	Robberto et al. (2013)	HST WFPC2	F336W	
37	Robberto et al. (2013)	HST WFPC2	F439W	
38	Robberto et al. (2013)	HST WFPC2	F656N	
39	Robberto et al. (2013)	HST WFPC2	F814W	
40	Robberto et al. (2013)	HST NICMOS	F110W	
41	Robberto et al. (2013)	HST NICMOS	F160W	

Table 1: Description of the columns in the optical to infrared photometry table

Column Index	Source Catalogue	Instrument	Filter	Comments
42	Lucas et al. (2005)	FLAMINGOS 1	K	
43	Lucas et al. (2005)	FLAMINGOS 1	H	
44	Lucas et al. (2005)	FLAMINGOS 1	J	
45	Robberto et al. (2005)	UKIRT MPIA	N	
46	Robberto et al. (2005)	UKIRT MPIA	N	
47	Robberto et al. (2005)	UKIRT MPIA	N	
48	Robberto et al. (2005)	UKIRT MPIA	Q	
49	Getman et al. (2005b)	Various	V	
50	Getman et al. (2005b)	Various	I	
51	Getman et al. (2005b)	Various	V	
52	Getman et al. (2005b)	Various	V	
53	Getman et al. (2005b)	VLT ISAAC	J	
54	Getman et al. (2005b)	VLT ISAAC	H	
55	Getman et al. (2005b)	VLT ISAAC	Ks	
56	Getman et al. (2005b)	VLT ISAAC	Lprime	
57	Getman et al. (2005b)	Various	V	
58	Getman et al. (2005b)	Various	I	
59	Getman et al. (2005b)	2MASS	J	
60	Getman et al. (2005b)	2MASS	H	
61	Getman et al. (2005b)	2MASS	Ks	
62	Hillenbrand et al. (1998)	Various	J	
63	Hillenbrand et al. (1998)	Various	H	
64	Hillenbrand et al. (1998)	Various	K	
65	Hillenbrand et al. (1998)	Various	L	
66	Hillenbrand et al. (1998)	Various	M	
67	Hillenbrand et al. (1998)	Various	N	
68	Hillenbrand et al. (1998)	Various	Q	
69	Feigelson et al. (2002)	Various	V	
70	Feigelson et al. (2002)	Keck NIRC	H	
71	Feigelson et al. (2002)	Keck NIRC	H	
72	Lada et al. (2004)	VLT ISAAC	Lprime	
73	Getman et al. (2005a)	2MASS	J	
74	Getman et al. (2005a)	2MASS	H	
75	Getman et al. (2005a)	2MASS	Ks	
76	Getman et al. (2005a)	Various	V	
77	Getman et al. (2005a)	Various	I	
78	Hillenbrand & Carpenter (2000)	Keck NIRC	H	
79	Hillenbrand & Carpenter (2000)	Keck NIRC	K	
80	Hillenbrand (1997)	Various	I	
81	Hillenbrand (1997)	Various	V	
82	Smith et al. (2005)	Gemini T-ReCS	Si-5	

Table 2: Description of columns in the submillimeter photometry table

Column Index	Source Catalogue	Instrument	Wavelengths
0	Mann et al. (2014)	ALMA	856 μ m
1	Mann & Williams (2010)	SMA	856-882 μ m
2	Mann & Williams (2010)	SMA	856-882 μ m
3	Mann & Williams (2010)	SMA	1338 μ m

3 Spectral Energy Distributions

3.1 Scripts

Creating the SEDs of proplyds contained in the source catalogue is done in numerous steps. The data must first be extracted from their respective photometric catalogues. The objects in these catalogues must then be cross identified with the proplyd catalogue by choosing the object nearest the proplyd within 2 arcseconds. The J2000 equatorial coordinate system is used in all the collected catalogues. The astrometric shift between the matched objects and the proplyds are then calculated. This shift of each catalogue table is then subtracted from its coordinates. Using these corrected coordinates the catalogues are cross identified again. This shifting and cross identifying is done three times. A visual inspection is then performed to compare the locations of the matched objects and proplyds. If an object was matched incorrectly it is removed from the list of each proplyd's matched object. The photometry from these catalogues for each proplyd is then put into a table. Proplyds with multiple measurements in the same band use all points. The magnitudes in this table are then corrected for extinction and converted to an energy density. This energy density is then plotted against wavelength to create the SEDs. Figure 2 depicts this work flow. The steps to calculate the variability are described in more detail in section 4.1.

3.1.1 Importing and extracting data

In order to create the SEDs, the data must first be extracted from the various catalogues. This is done in two steps, the first step is contained in `info_import.py`. The Python script `info_import.py` first reads the `readme` file for each catalogue in order to find the `byte-by-byte description` for each table in the catalogue. This `byte-by-byte description` is a table which contains 5 columns which are read into the program. The first column contains the starting and ending byte of a column in the data table which is used to calculate the column width in the data table which is needed in the next step. The last column in the `byte-by-byte description` contains a short explanation of the contents of the column and which string is used to indicate an unknown value. This script writes 4 files to the `./pickles` directory. They are: `keys.p`, `info2.p`, `f1.p`, and `tabnames.p`. These files contain the keys to access the dictionaries which contain the data for each catalogue table, a dictionary containing the column descriptions for each catalogue table, the file list which contains the names of the compressed *VizieR* archives, and the names of each table in each catalogue respectively. The keys for each dictionary consist of a string of five characters where the first two characters are the catalogue number, starting at zero, and the last two characters are the table number in the `Readme` starting at zero. For example `08_01` is the key for catalogue 8 table 1. This corresponds to *Table 5: ACS Source Catalog* in *The Hubble Space Telescope Treasury Program on the Orion Nebula Cluster* by Robberto et al. (2013).

The second step is to extract the data from the data tables. This is done in

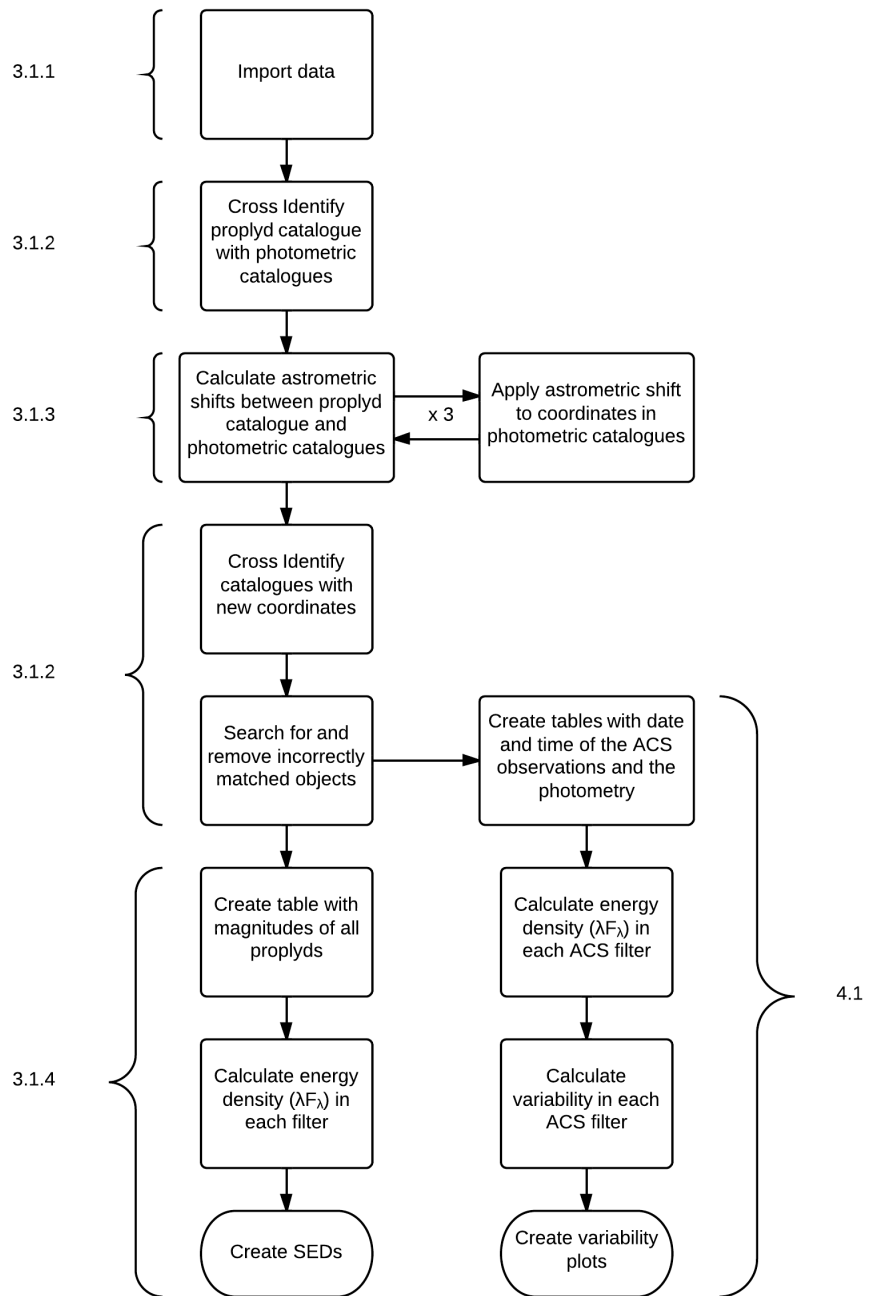


Figure 2: Flowchart of the work flow of this work.

`extract_data.py` by using the column widths for each table from the previous step. Once this is done the data for each table is stored in a dictionary using the same keys as the previous step. The tables are then scanned for values which indicate unknown values, these values are replaced with NaN so that calculations in the next steps can continue uninterrupted. These NaN values can be easily found in tables later on and removed during plotting. This script also searches for flags which indicate upper limits for fluxes. The tables from *Circumstellar Disks in the Orion Nebula Cluster* by Hillenbrand et al (Hillenbrand et al. 1998) are updated to the 2001 version³ of the table in this script. Three files are written to the `./pickles` directory: the updated versions of `keys.p`, `info2.p`, and `data.p`, respectively. The last file is a dictionary which contains all the tables for all the catalogues. From here on the dictionaries `info2` and `data` are not changed.

3.1.2 Cross-identification and correcting for astrometric shifts

After importing the data from the tables, the catalogues must be crossmatched with each other using `crossid.py`. Before this is done, all the coordinates in the tables must be converted from sexagesimal to degrees. They are then put into a dictionary and adjusted for differences in astrometry using `astrometry.py`. The adjusted coordinates are used to calculate the separation between the proplyds in Ricci et al. (2008) and the selected objects in the other catalogues. If the separation is less than two arcseconds, the object is added to a list of key-table indices. However, some of the proplyds are close to other objects and this crossmatching may have selected an incorrect object as a proplyd. Using *SAOImage DS9*⁴ and the F775W *HST ACS* mosaic of the Orion Nebula, a visual inspection is done to compare the location of the Ricci et al. (2008) coordinates and the catalogue coordinates. For proplyds where the incorrect objects were matched, the incorrect objects were added to a list and then removed from the list containing the proplyds and the crossmatched catalogues. Each proplyd now has a list of key-indices and table-indices which allow the correct line from each table to be selected. Two new files are created; `proplyds.p`, and `coordsd.p`. They contain the crossmatched and checked list of proplyds and catalogues, and a dictionary of the coordinates of each object in each catalogue respectively.

Once the crossmatching is completed, `ds9regions.py` creates files which can be read into *DS9* and overlaid onto the mosaic of the Orion Nebula. A shift between the image coordinates and the catalogue coordinates is accounted for in this script. This shift was calculated by taking the coordinates of 8 proplyds from Ricci et al. (2008) and from the mosaic. These proplyds were distributed all over the field of the mosaic. The shift was calculated using the same method as `astrometry.py`, which is discussed in section 3.1.3.

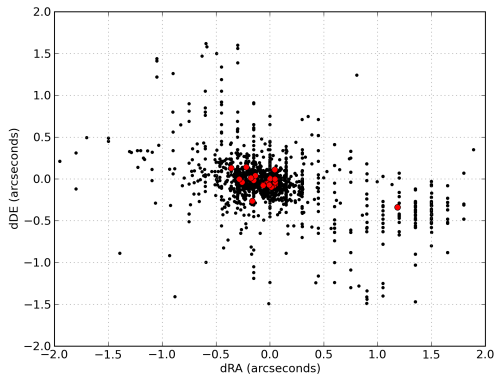
³Available at www.astro.caltech.edu/~lah/papers/orion_disks.table1a.working

⁴<http://ds9.si.edu>

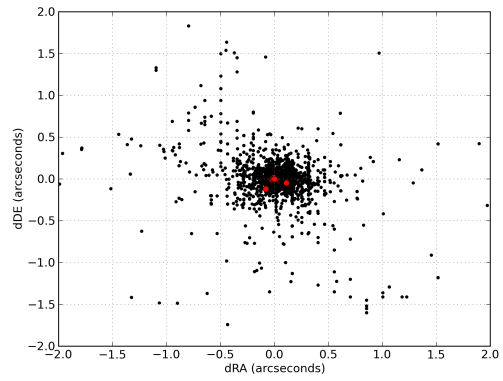
3.1.3 Astrometric shift in catalogue tables

After the first crossmatching `astrometry.py` is run. This takes the RA and DEC coordinates for each matched object and calculates the separation vector to its proplyd. This separation vector is then averaged over the proplyds in each catalogue table such that the average astrometric shift is calculated for each catalogue table compared to the Ricci et al. (2008) catalogue. This shift is then corrected for in `crossid.py` by adding the shift for each catalogue table to the coordinates of all the objects in that catalogue table. After this, `crossid.py` is ran again using the shifted coordinates. This is done three times as some different objects are matched after the first correction. These improvements in astrometry can be seen in figure 3, where the black dots are the separations between an object and its matched proplyd, and the red dots are the average separations between an object and its matched proplyd in each catalogue table. The maximum object separation decreases each time `astrometry.py` is run. The root mean square separation decreasing from 0.42 arcseconds in figure 3a to 0.24 arcseconds in figure 3d. The final shifts in the coordinates of the catalogue tables compared to those of Ricci et al. (2008) can be seen in table 3.

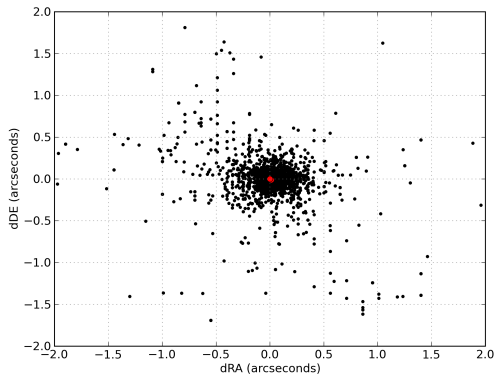
After the corrected crossmatching is completed `coalesce.py` is run. All the data from each catalogue for each proplyd is put into rows of a table. The descriptions of the columns of all the catalogue tables are searched for magnitudes and their errors. The columns which contain magnitudes or fluxes are inserted into a table with each row belonging to a proplyd. The same is done for the errors of these columns and upper limits. These tables are then written to disk in five files. A list containing a table of all the columns in all the catalogue tables for each proplyd, a list with the descriptions of each of these columns, and a list with the descriptions of the columns containing magnitudes or fluxes. This list is contained in `propdat_coal.p`. The next file, `propdat_proplyds.p`, contains an updated list of proplyds and their matched catalogue objects. Subsequently, `propinfo_magdmag.p`, contains the table for the magnitudes and fluxes for each proplyd and a table for the errors associated with them. The next file, `propinfo_limit.p`, contains the flags for limits for each object in the previous table.



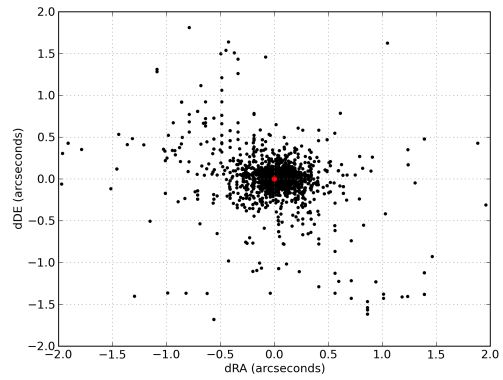
(a) Uncorrected for astrometric errors.



(b) Corrected once for astrometric errors.



(c) Corrected two times for astrometric errors.



(d) Corrected three times for astrometric errors.

Figure 3: Separation between matched object and proplyd. Black dots represent matched objects, red dots represent the mean inside one catalogue table.

Table 3: Shifts in coordinates of catalogue tables compared to those of Ricci et al. (2008) in arcseconds

Catalogue	Catalogue Index	Table Index	dRA	dDE
Cutri & et al. (2012)	0	0	-0.241	-0.382
Robberto et al. (2010)	3	0	-0.091	-0.082
Kryukova et al. (2012)	4	0	0.049	-0.063
Da Rio et al. (2010)	5	0	-0.029	-0.052
Da Rio et al. (2012)	6	0	-0.012	-0.043
Da Rio et al. (2009)	7	0	0.049	-0.083
Da Rio et al. (2009)	7	1	0.050	-0.040
Da Rio et al. (2009)	7	2	0.013	-0.096
Robberto et al. (2013)	8	1	0.006	-0.078
Robberto et al. (2013)	8	2	0.002	0.003
Robberto et al. (2013)	8	3	-0.358	0.131
Lucas et al. (2005)	9	0	-0.062	-0.079
Robberto et al. (2005)	10	0	-0.219	0.143
Getman et al. (2005b)	11	0	-0.257	-0.038
Hillenbrand et al. (1998)	12	0	1.311	-0.398
Feigelson et al. (2002)	13	0	-0.169	-0.018
Lada et al. (2004)	15	0	-0.136	0.039
Smith et al. (2005)	16	0	0.046	-0.002
Hillenbrand & Carpenter (2000)	18	0	-0.184	0.005
Hillenbrand (1997)	19	0	1.311	-0.398
Hillenbrand (1997)	19	1	1.311	-0.398
Mann et al. (2014)	20	0	-0.284	-0.002

3.1.4 Manipulating Data

Once all the previous steps have been completed `proc_data2.py` is run. The script first searches for V-band extinction in the imported catalogue tables and creates a list of proplyds and their extinction from multiple catalogues. After this a new table is created from `propdat_raw.p`, where only the magnitudes or fluxes are kept. The same is done for the errors in the magnitudes or fluxes. A table containing the effective wavelength and the zeropoint flux of all the filters used by all the catalogues is then created. These tables are needed to convert the observed magnitudes to fluxes. If the flux densities are in Janskies (F_ν) they are converted to F_λ using the following equation:

$$F_\lambda = 10^{-23} \times \frac{c F_\nu}{\lambda^2} \quad (1)$$

Where F_λ is the flux density as a function of wavelength, c is the speed of light, F_ν is the flux density as a function of frequency in Janskys, and λ the wavelength of the flux density.

The previously created table is then cleared of values which are not numbers or are unknown. At this time the code searches for flux upper limits for the flux densities. From the table of extinctions, an extinction is selected for each object. This selection is done as follows: if an extinction is available from Da Rio et al. (2012) it is used, and if it is negative the next available extinction is searched in Da Rio et al. (2010). Otherwise Hillenbrand (1997) is used. If a proplyd has no extinction available then an extinction of 1.5 magnitudes is used as it is the median interstellar extinction for bodies in the Orion Nebula (Da Rio et al. 2010). Once this is done the extinction for each filter is calculated using the Cardelli Extinction Law (equation 2a) (Cardelli et al. 1989) with $R_V = 3.1$.

$$\frac{A_\lambda}{A_V} = a(x) + \frac{b(x)}{R_V} \quad (2a)$$

$$x = \frac{1}{\lambda}, \quad 0.3\mu\text{m}^{-1} < x < 3.3\mu\text{m}^{-1} \quad (2b)$$

Where A_λ is the extinction at λ , A_V is the extinction in the V-band, $a(x)$ and $b(x)$ are polynomials dependent on whether λ is in the UV, optical to near-infrared, or infrared. These polynomials are available in full in the paper by Cardelli et al. (1989). This law extinction gives the ratio of extinction at wavelength λ to the extinction in the V-band. The magnitudes for each proplyd are then de-reddened and converted to a flux. After this, the submillimeter fluxes are manipulated to create 3 tables which contain the flux, the error in flux, and the wavelength of the flux, respectively. The error in magnitude of the proplyds from some catalogues have to then be added manually as they are not in the catalogue tables. In these cases the error is taken to be constant in the catalogue as mentioned in the accompanying paper. Before the SEDs can be plotted each instrument must have its own marker so it can be easily identified on the SEDs. These markers consist of 6 different shapes in 4 different colours. The markers for *HST* are red so that it can be easily identified, and the markers for PSF and aperture photometry in Robberto et al. (2010) are also differentiated between. A function to plot the SEDs is created. This function converts the flux densities to energy densities and removes any NaNs from the list of energy densities for each object. To calculate the energy density for a filter the following equation is used:

$$\lambda F_\lambda = \lambda \times F_0 \times 10^{-0.4 \times (m_f - A_f)} \quad (3)$$

Where λ is the central wavelength of the filter, F_0 is the zeropoint flux of the filter, m_f is the observed magnitude in the filter, and A_f is the extinction in the filter. The cleaned list is then plotted against wavelength on a log-log plot to create the SED. There are a few catalogues of spectral types available. The most recent spectral type catalogue is by Hillenbrand et al. (2013). If a spectral type is available, the blackbody curve of the effective temperature corresponding to that spectral type is then plotted on the SED using equation 4, where h is the Planck constant, c is the speed of light in a vacuum, k is the Boltzmann constant, λ is the wavelength, and T is the effective temperature for that spectral type.

$$\lambda B_\lambda = \frac{2hc^2}{\lambda^4} \frac{1}{e^{\frac{hc}{\lambda kT}} - 1} \quad (4)$$

A scaling is also applied to shift the calculated blackbody curve to the correct position on the SED (eq 5). This is done by averaging the shift between the blackbody model and the points on the SED. The filters used to calculate this shift had a central wavelength between 0.4 μm and 0.7 μm . The H α filters were excluded from this selection.

$$K = \frac{1}{N} \sum \log_{10} \frac{\lambda B_\lambda}{\lambda F_\lambda} \quad (5)$$

Where N is the number of points used to calculate the shift, λB_λ is the blackbody energy density at wavelength λ , and λF_λ is the energy density at wavelength λ . This constant K changes for each proplyd.

Subtracting equation 5 from the logarithm of equation 4 results in equation 6 which is the plotted function y .

$$y = \log_{10}(\lambda B_\lambda) - K \quad (6)$$

The plots are accompanied by images of the proplyd in the ACS filters. The scaling of these images is logarithmic in order to bring out faint structures. This script also writes five tables to disk. `Flam.csv` contains the energy density of each proplyd in each filter, whilst `err_Flam.csv` contains the errors associated with those fluxes. `wavelength.csv` contains the central wavelengths of the filters for these energy densities. Similarly, `Flam_mm.csv` and `err_Flam_mm.csv` do the same thing but for the submillimeter data. Finally, `wavelength_mm.csv` is also written to disk as the wavelengths of the submillimeter data can vary for each observation.

3.2 SEDs

In the following section the SEDs for a selection of proplyds are shown. This selection consists of four main types of proplyd: ionized objects (figures 5,6,7,8, respectively), pure silhouettes (figure 9), reflection nebulae (figure 10), and jets (figure 11). The ionized objects type consists of four sub-types which are described in section 3.2.1. These types tell whether a star or disk is visible inside the cocoon of the proplyd. This work is the first which attempts to create the SEDs of, and classify proplyds in the Orion Nebula according to their SEDs using photometry available in the literature. The legend for each of the following SEDs is shown in figure 4. The images accompanying the SEDs have a field of view of around $6'' \times 6''$. In these images North is up and East is left. The scaling for the images accompanying is shown in equation 7, where $I_{i,j}$ is the scaled pixel value at location i, j , $U_{i,j}$ is the unscaled pixel value at location i, j , and U_{\max} and U_{\min} are the maximum and minimum pixel values in the image respectively. Pixels where $U_{i,j}$ is equal to zero are ignored.

$$I_{i,j} = \frac{\log_{10}(U_{i,j}/U_{\min})}{\log_{10}(U_{\max}/U_{\min})} \quad (7)$$

Above the SEDs there is some information about the depicted proplyd; 'id' is the index of the object in this work, starting at 0 and going up to 218, 'name' is the name of the object in the Ricci et al. (2008) source catalogue, 'Av' is the used V-band extinction. For type, the letters mean the following; i: ionized disk seen in emission; d: dark disk seen only in silhouette; rn: reflection nebulae with no external ionized gas emission; j: jet emission with no evidence of either ionized disk or silhouette disk, J: jet; RN: reflection nebula; EO: disk seen nearly edge-on; FO: disk seen nearly face-on; B: binary system (Ricci et al. 2008). Finally, 'spec type' is the spectral type given by Hillenbrand et al. (2013). It is used to plot a blackbody curve on the SED.

The catalogue by Robberto et al. (2013) provides photometry performed in both drizzled and undrizzled ACS images. If both are available, the photometry on the drizzled images is selected first because these are free of cosmic rays and other instrumental artifacts. On the SEDs they can be differentiated by their markers (figure 4). In some SEDs the WFPC2 energy densities are higher than the ACS energy densities. This is due to the different aperture sizes used in the photometry. WFPC2 typically uses apertures that are around twice as large as those from ACS. For SEDs where submillimeter data was available the x-axis uses a different range than when it is not available.

The classification of proplyds is done in the $H\alpha$ image. The reason for this is that for many objects with no star visible in $H\alpha$ the star starts to appear in the F775W and F850LP images.

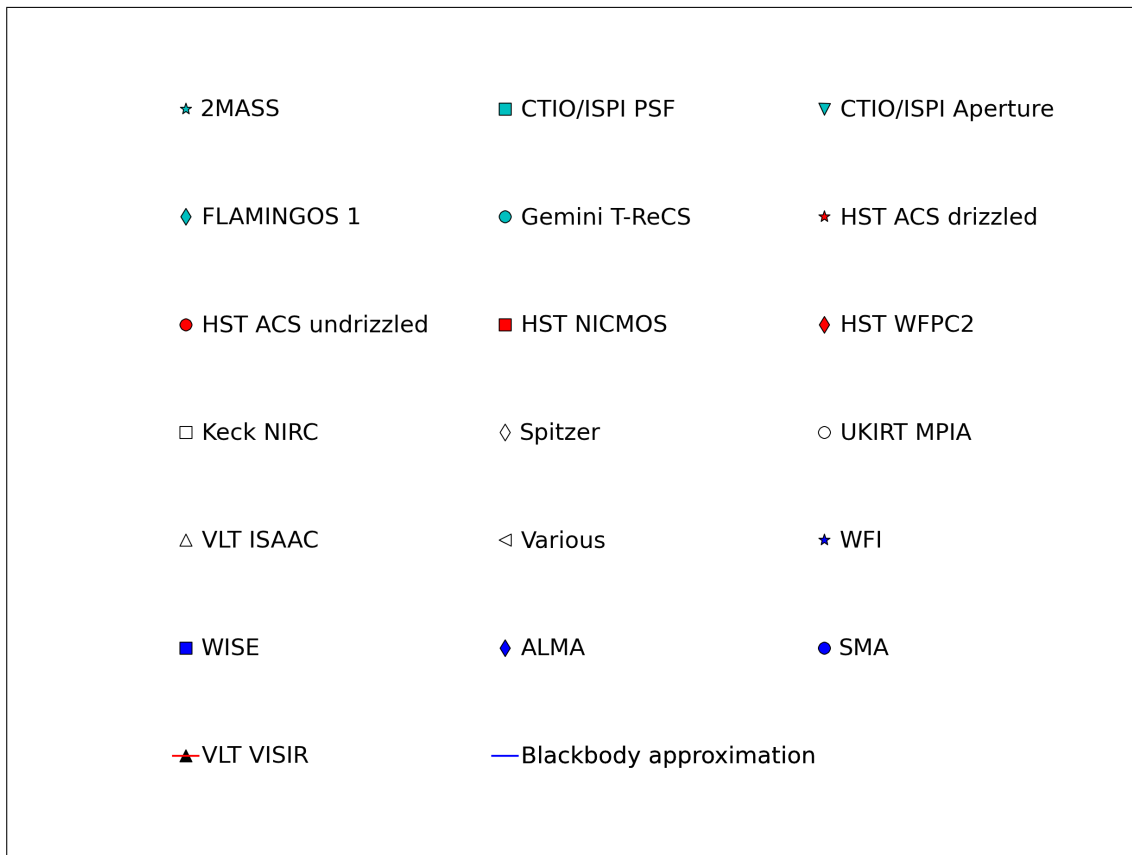


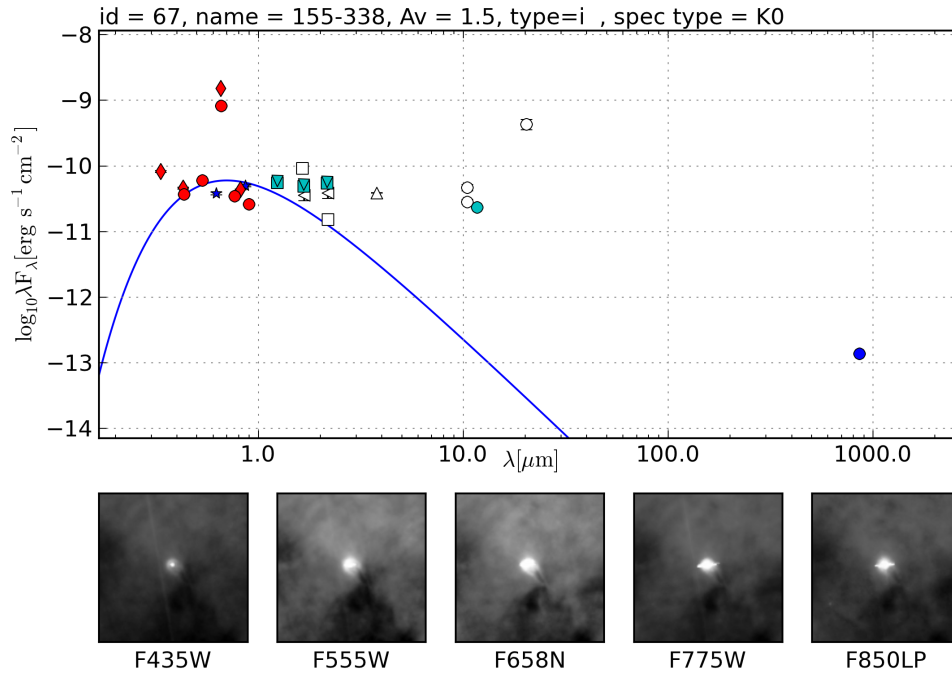
Figure 4: Legend for SEDs produced by this work.

3.2.1 Ionized objects

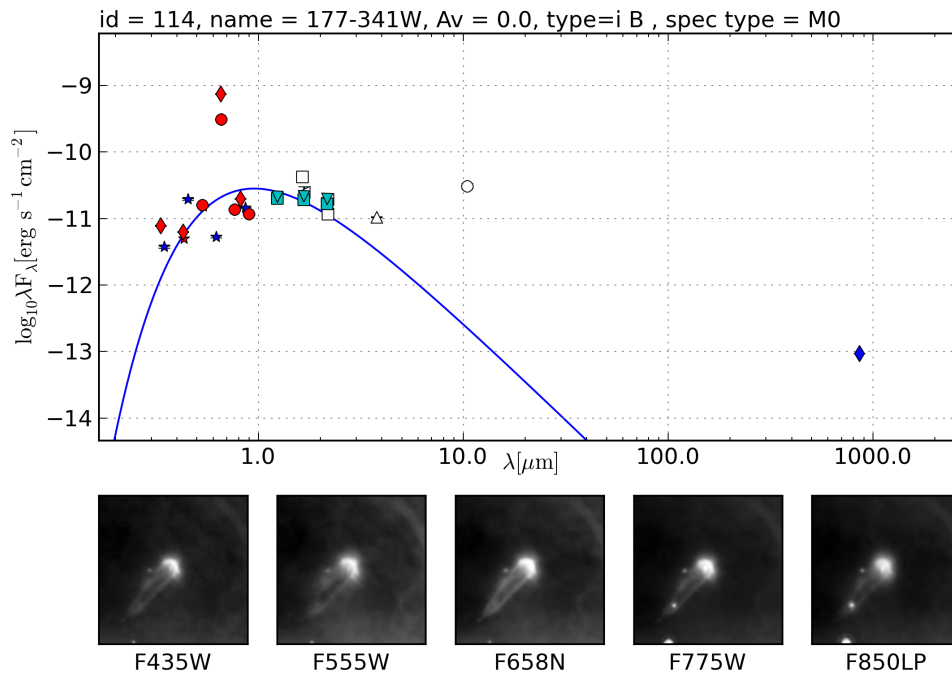
In this work ionized objects refer to objects where a tear drop shaped cocoon is visible in one of the accompanying images.

3.2.1.1 No star or disk visible inside cocoon

Figure 5 shows two proplyds where the star or disk inside the cocoon is not visible. The cocoon is clearly visible and there is a bright ionization front visible at the head of the proplyd. They both point towards the bright Trapezium stars. Both SEDs have a spike of around one order of magnitude in the $H\alpha$ filters. This is to be expected as the proplyds have bright ionization fronts and are separated by around $25''$ from θ^1 Ori C. Both proplyds have a clear infrared excess. Both SEDs are relatively flat, however 155-338 turns up sharply after $10\mu\text{m}$. Proplyd 177-341W has a slight dip around $4\mu\text{m}$.



(a)

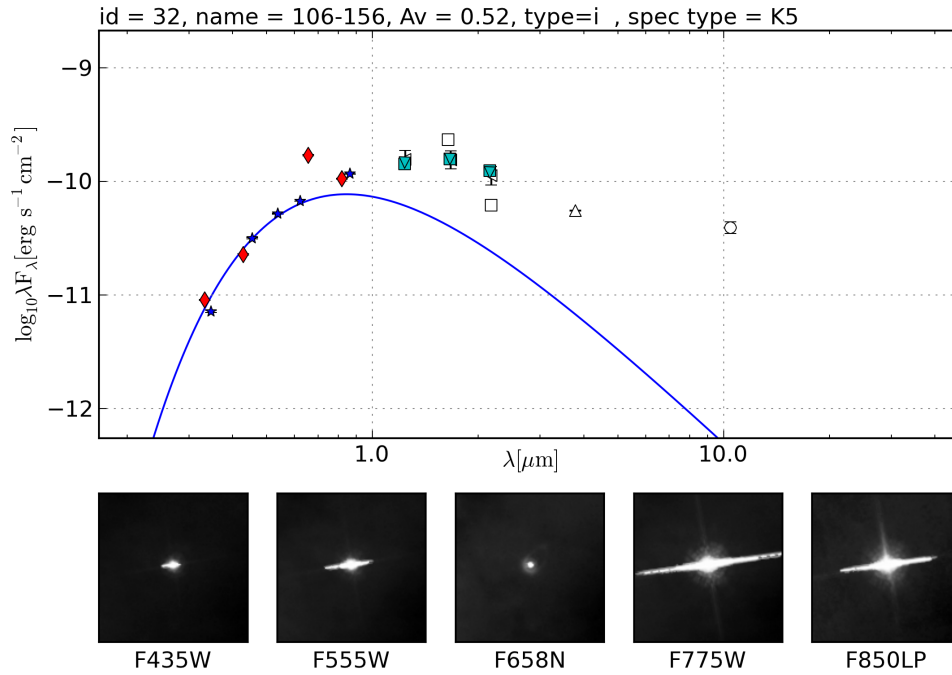


(b)

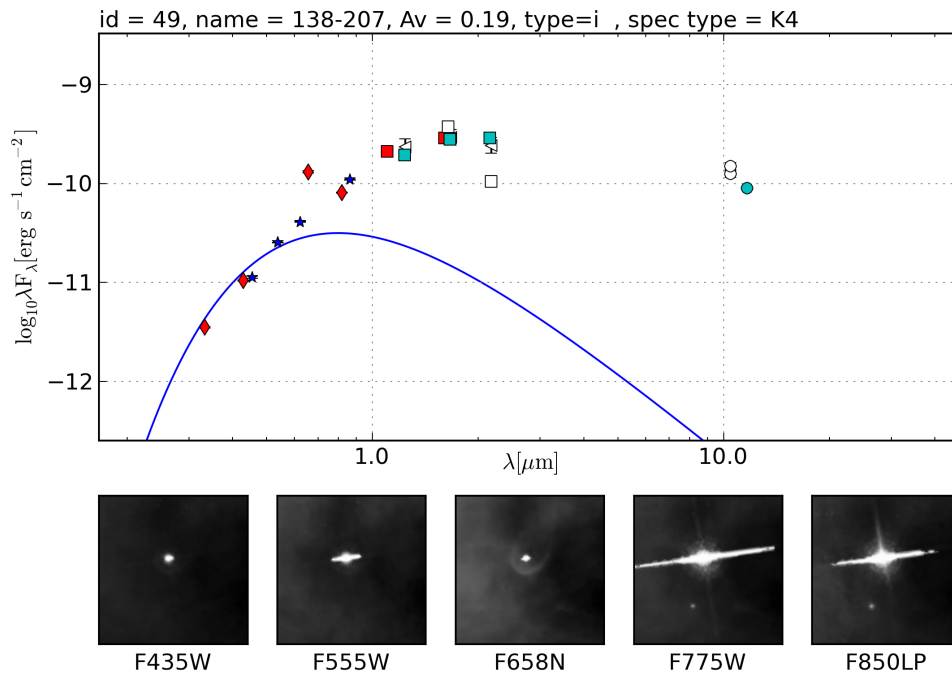
Figure 5: No star or disk visible inside cocoon

3.2.1.2 Only star visible inside cocoon

Figure 6 shows two proplyds where the central star is visible inside a cocoon. They both have a slight bump in $H\alpha$. Proplyd 106-156 is at a projected distance of $120''$ to θ^1 Ori C, and 138-207 at $85''$. Excluding the $H\alpha$ filter, both proplyds peak in the H-band. Both proplyds show an infrared excess, however that of 106-156 is less pronounced than the excess shown by 138-207. It appears that 106-156 starts to curve up again at around $4\mu\text{m}$, 138-207 does not have this data point so it is not possible to tell.



(a)

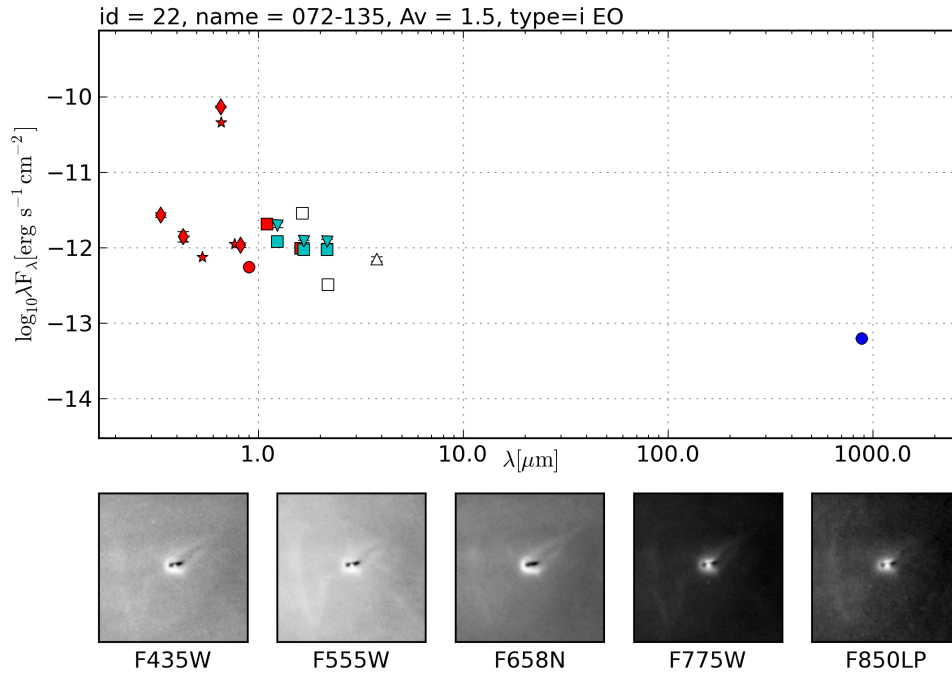


(b)

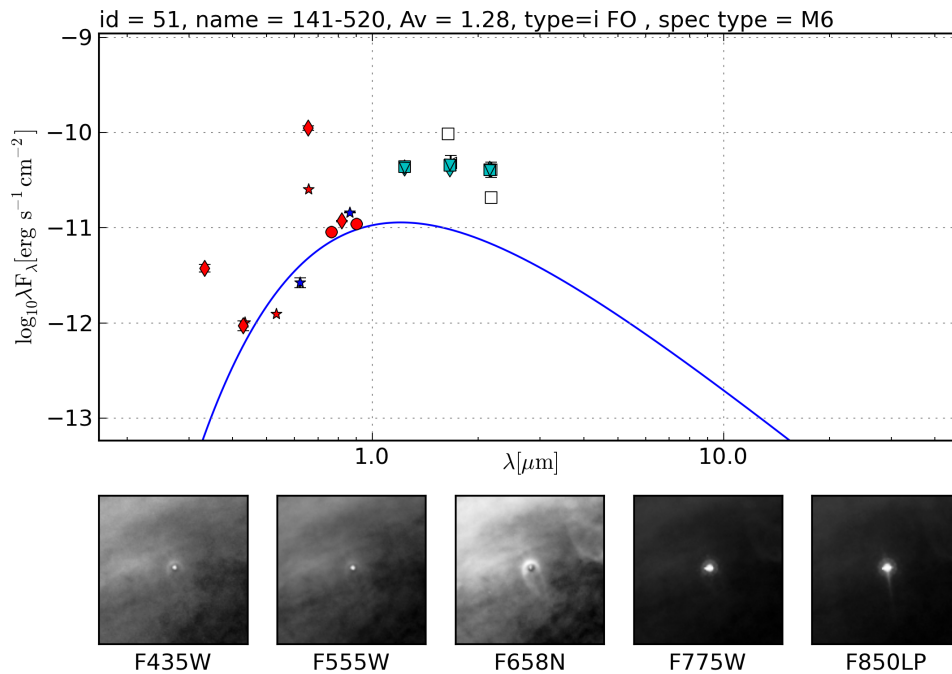
Figure 6: Only star visible inside cocoon

3.2.1.3 Star and disk visible inside cocoon

Figure 7 shows two proplyds where the star and disk are both visible inside the cocoon. The disk is visible as it is silhouetted over the bright nebular background. Proplyds 072-135 and 141-520 have large $H\alpha$ contributions even though they are at a projected distance of 180'' and 120'' respectively to θ^1 Ori C. At wavelengths less than $0.6\mu\text{m}$ 072-135 slopes down steeply. The general shape of these SEDs is a downward slope at the shorter wavelengths, then rising again until the near infrared.



(a)

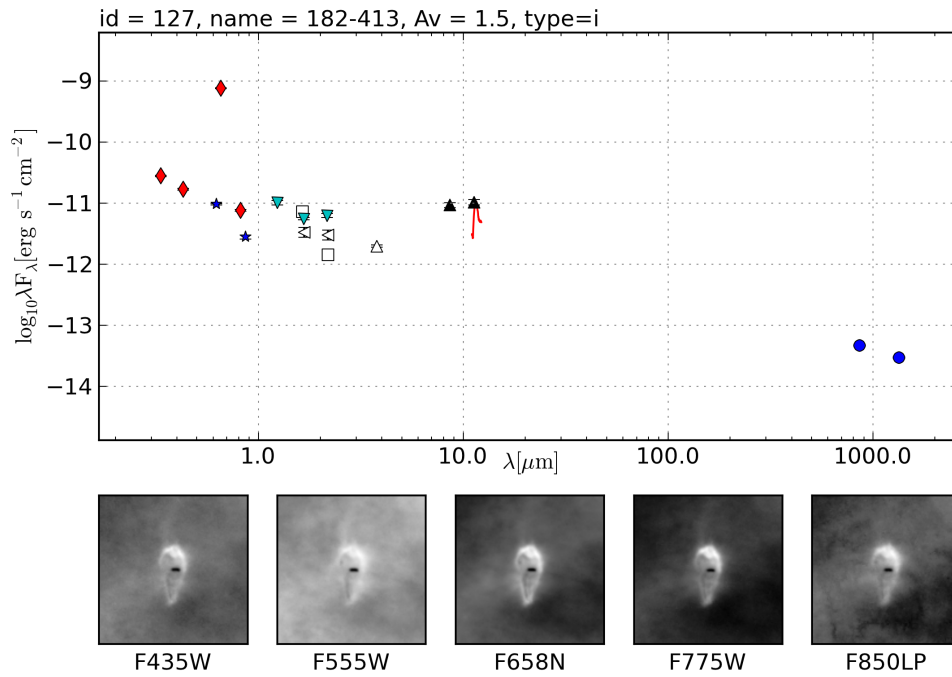


(b)

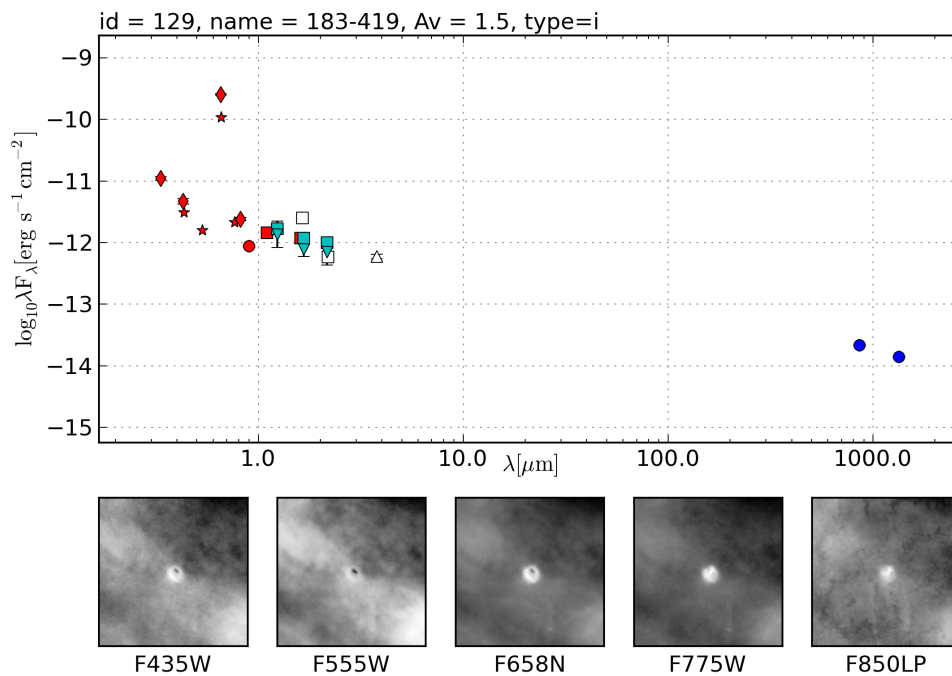
Figure 7: Star and disk visible inside cocoon

3.2.1.4 Only disk visible inside cocoon

Figure 8 shows two proplyds where only the disk is visible as an embedded silhouette inside a cocoon. Both proplyds have a large peak in $H\alpha$. They have a projected distance of around $60''$ to θ^1 Ori C. They both have a general downward sloping trend. Proplyd 182-413 slopes up again in the mid infrared. In the submillimeter there is a downward trend. The red line in figure 8a is a spectrum obtained with VISIR on the *VLT*.



(a)

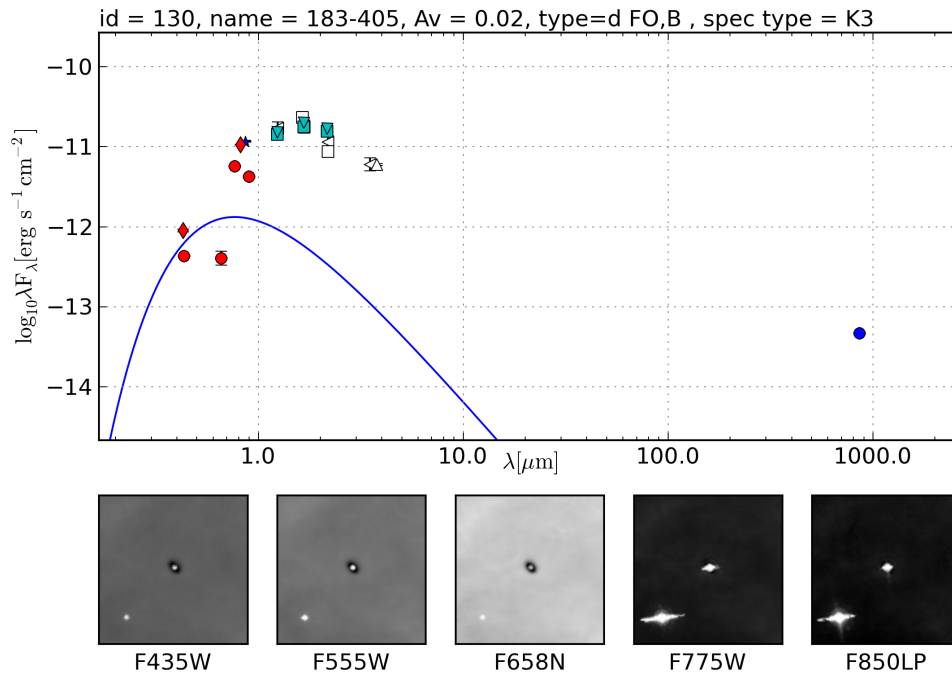


(b)

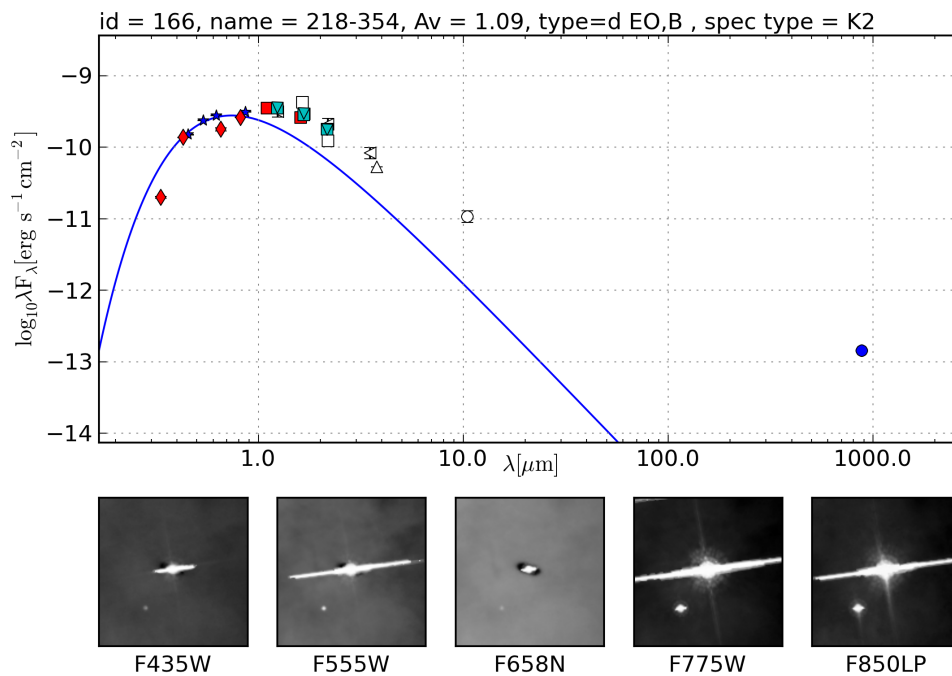
Figure 8: Only disk visible inside cocoon

3.2.2 Pure silhouettes

Figure 9 shows two proplyds where a disk is silhouetted against the brighter nebulous background. Both 183-405 and 218-354 show no $H\alpha$ and are at a projected distance of 50'' and 90'' to θ^1 Ori C, respectively. Both SEDs slope down after around $1\mu\text{m}$. However, 183-405 shows a significant infrared excess, whilst 218-354 shows only a slight infrared excess.



(a)

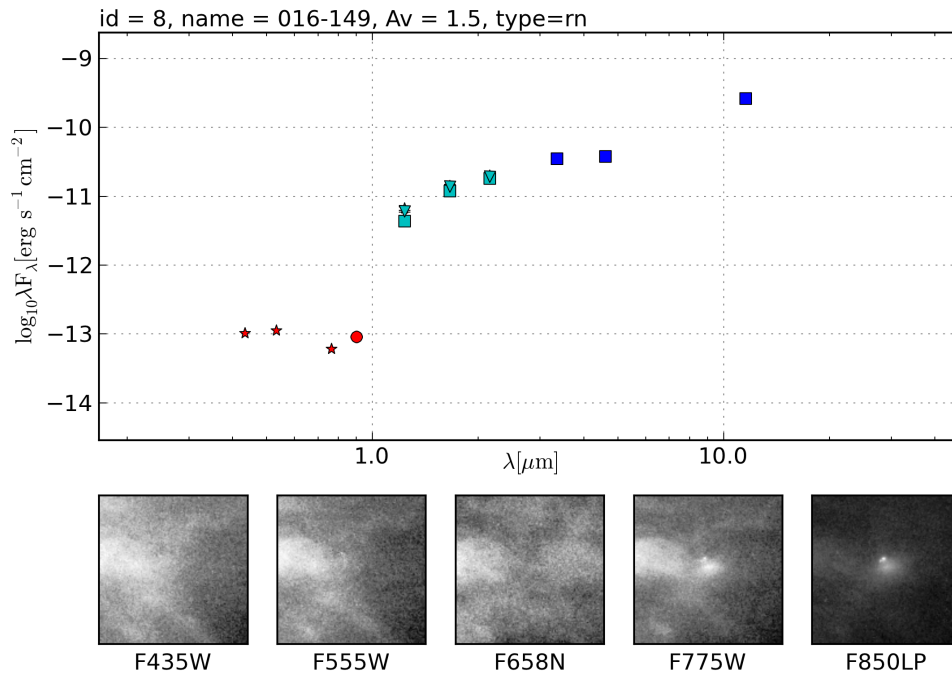


(b)

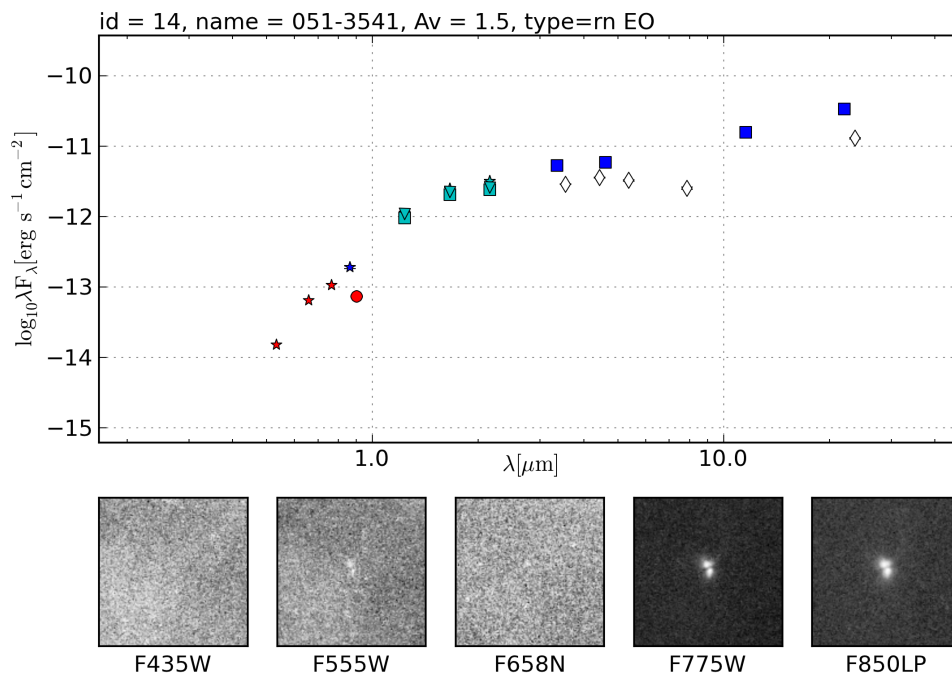
Figure 9: Pure silhouettes

3.2.3 Reflection Nebulae

Figure 10 shows two reflection nebulae which show a dark lane across polar emission. Both reflection nebulae do not show any $H\alpha$ emission as can be seen from the images. They only become visible at longer wavelengths. Both 016-149 and 051-3541 are relatively far away from bright OB stars. They are at a projected distance of 240'' and 760'' to θ^1 Ori C, respectively. Both SEDs have the same general shape with a decreasing positive slope until an increase in the slope between 5 and 10 μm . Both these objects use the median extinction from Da Rio et al. (2010).



(a)

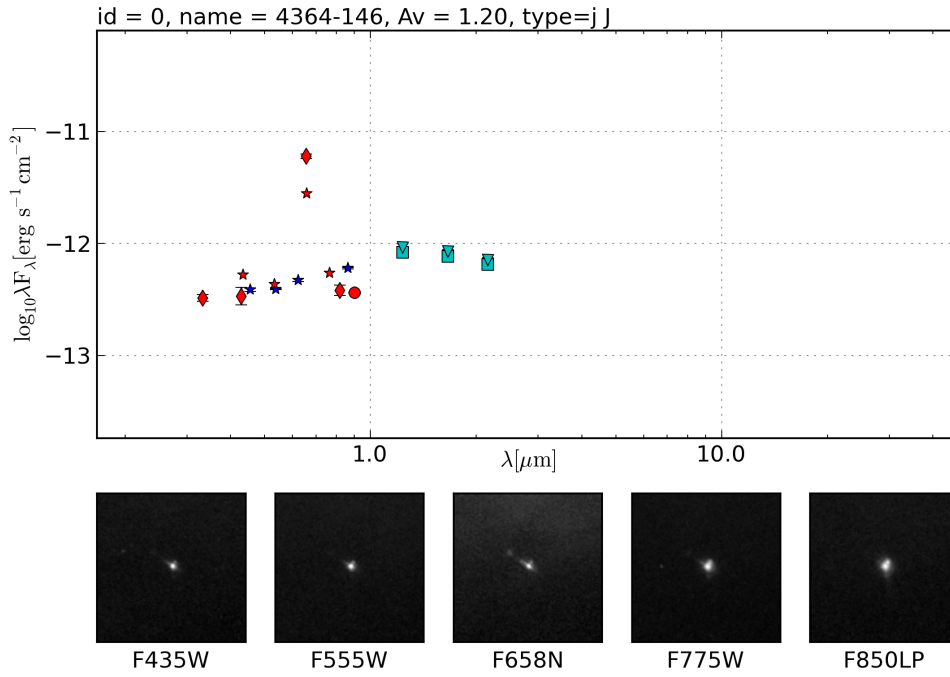


(b)

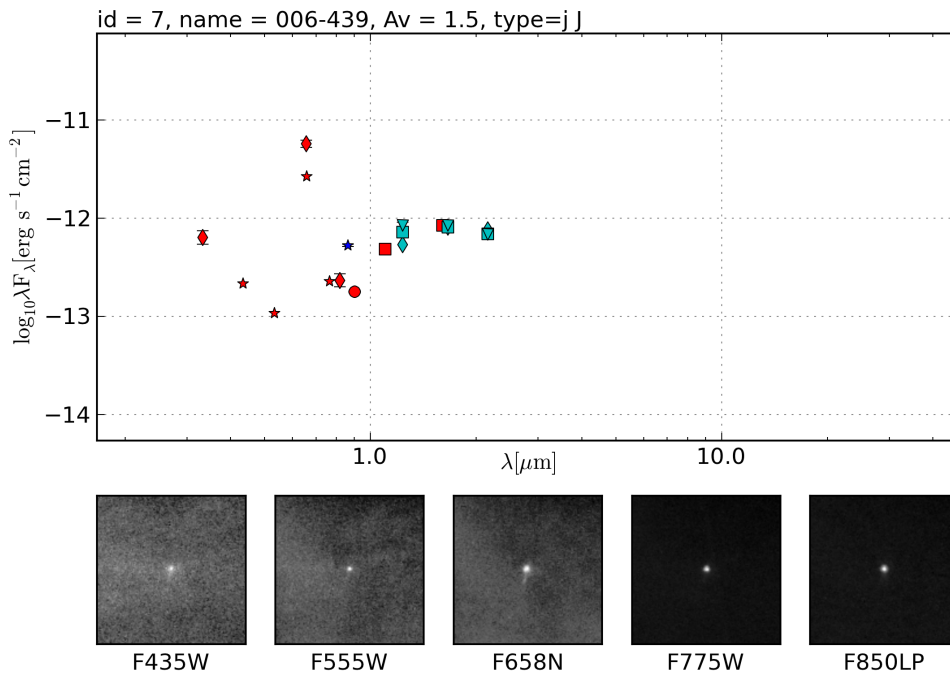
Figure 10: Reflection Nebulae

3.2.4 Jets

Figure 11 shows two objects with jets emanating from them. Both jets have an $H\alpha$ peak and no visible ionization front. The jets 4364-146 and 006-439 are at distances of 610'' and 250'' from θ^1 Ori C respectively. The SED of jet 4361-146 is very flat rising by only half an order of magnitude and peaking in the J-band. The SED of jet 006-439 on the other hand slopes down steeply in the optical before rising in the near infrared. Here too the median extinction of Da Rio et al. (2010) is used.



(a)



(b)

Figure 11: Jets

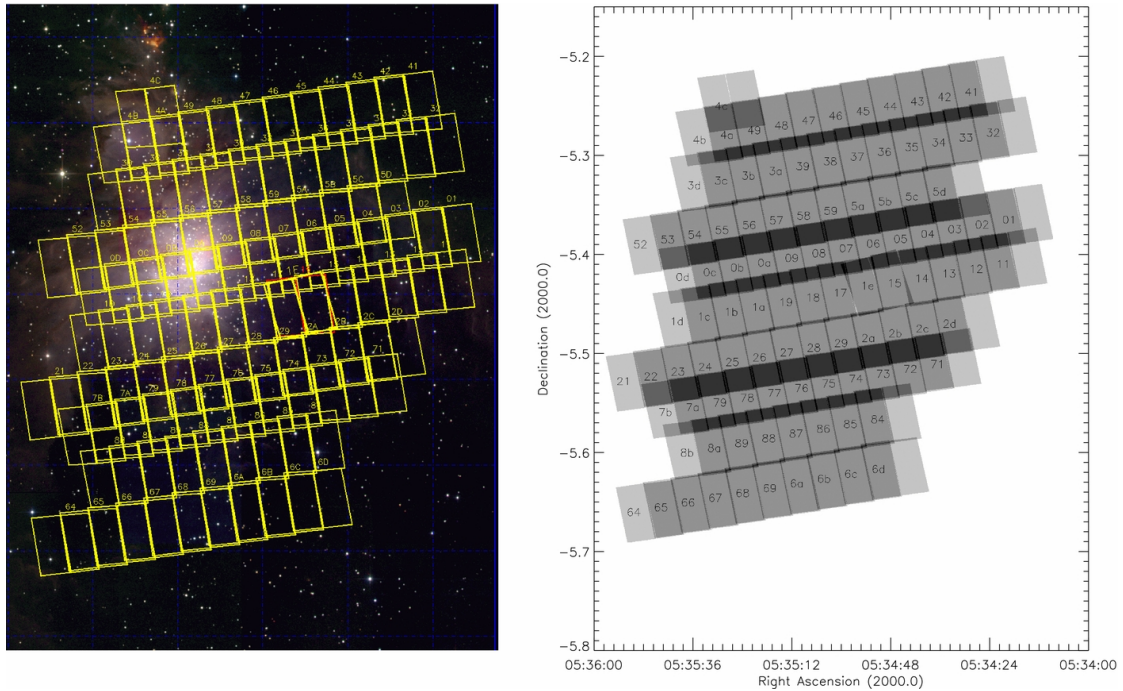


Figure 12: Total coverage of the ACS survey, superimposed to a color-composite JHK image of the Orion Nebula from 2MASS (left panel). The right panel highlights the overlapping regions between neighboring visits (darker gray shades), and reports the reference identification number of each of the individual visits. Figure and caption from Robberto et al. (2013)

4 Variability

The Treasury program on the Orion Nebula (Robberto et al. 2013) allows an investigation to be made into the variability. This is made possible due to the method in which the Orion Nebula was surveyed. The scanning pattern (figure 12) typically provides two images with ACS for each filter. However, there were a few exceptions in this as the half fields at the ends of each strip are covered by only one of the two ACS CCDs and so are observed only once. The regions between adjacent strips where the strips overlap are typically observed four times. A small fraction of the ACS field is observed one or three times due to detector gaps or due to repeated visits. The observations of the Orion Nebula were made over the course of a year. The shortest maximum time between observations was a little over 90 minutes, while the longest time between observations was a little over 1 year.

4.1 Script

In `variability.py` the variability of the proplyds in each filter of ACS is plotted. For each proplyd the script takes the objects which were matched in `crossid.py` with the proplyd from the *ACS* catalogue. It then searches for objects which

have exactly the same coordinates as those of the closest object. The script then searches for the date the objects were observed and the magnitude of the objects in the *ACS* filters. These magnitudes are then converted to an energy density without correcting for extinction i.e. using $A_f = 0$ in equation 3. The script also calculates the maximum change in the logarithm of these energy densities and plots a histogram of this value for each filter (figure 13). It also calculates the error in the logarithm of the energy densities and creates a histogram for these values for each filter as well (figure 14). Finally, it selects proplyds where the average variability in all the filters is greater than the maximum photometric error in any filter. The variability in this selection is then plotted against each filter, with the order of the filters being F435W, F555W, F775W, F850LP, F658N. Each line signifies one proplyd. The average variability in this selection and of all proplyds in each filter and plots these as red squares and black squares, respectively (figure 15).

4.2 Variability Plots

Presented are plots of the maximum change in the flux of each filter over the course of *ACS* observations (figure 13), the error in flux in each filter (figure 14), and the variability of each proplyd in each filter (figure 15). For figure 15 the proplyds which are plotted have a mean variability in all filters which is greater than the maximum photometric error in any filter. Figure 13 shows that there is clearly observed variability in the observed proplyds as there are many instances where the observed energy density in a filter is greater than the maximum photometric error in that filter. Figure 14 shows that the photometry for the observed energy densities is good, as the error in the logarithm of energy density is always less than 0.1 order of magnitude for each filter. Finally, figure 15 shows how the variability for a proplyd varies across different filters. The proplyds depicted are those with the highest variabilities. The highest average variability occurs in F435W and the maximum variability in F555W. Objects with high variabilities in the wide-band filters also show a high variability in the $H\alpha$ filter. The maximum timespan between two observations was a little over 1 year, whilst the minimum was 1.6 hours. Out of 201 objects with a calculated variability 133 of those had a maximum timespan of under 1 day, and 57 of under 6 hours. Such a short timespan gives very little time for a proplyd to display variability. The number of proplyds which display a variability greater than the maximum photometric error in filters F435W, F555W, F775W, F850LP, and F658N are 72, 56, 52, 90, 56, respectively. There are 57 proplyds which display an average variability across all filters greater than the maximum photometric error in any of the filters.

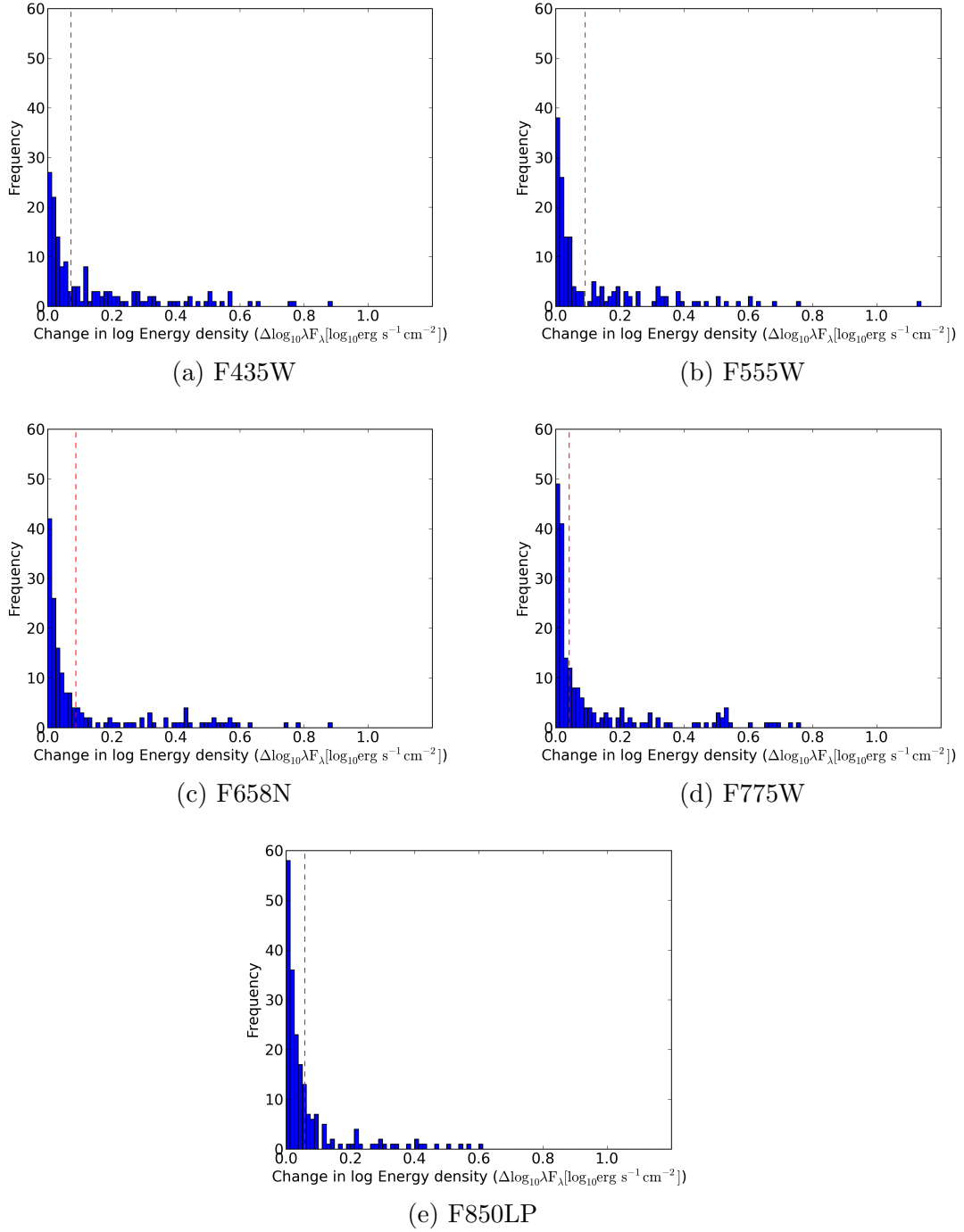
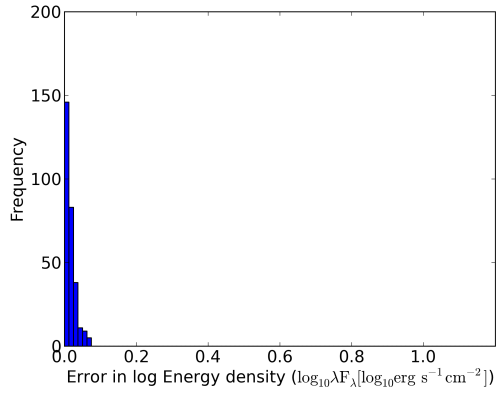
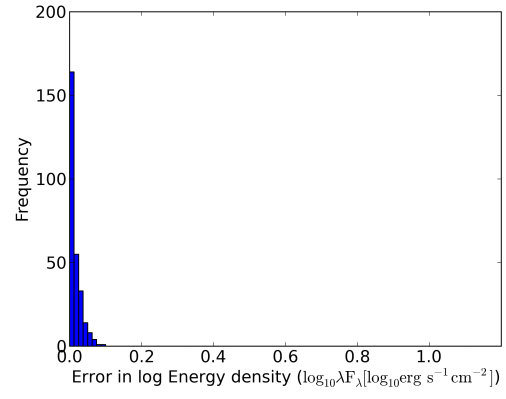


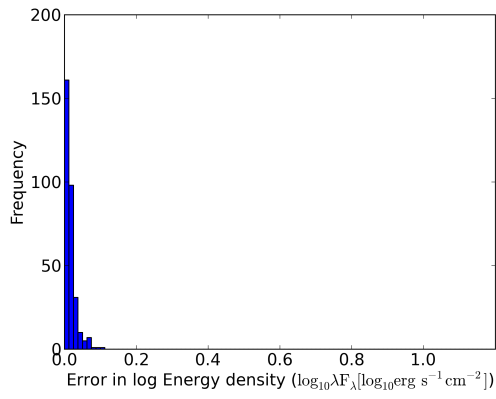
Figure 13: Maximum change in the energy density of each filter over the course of *ACS* observations. The vertical red dashed line is the maximum photometric error in the corresponding filter.



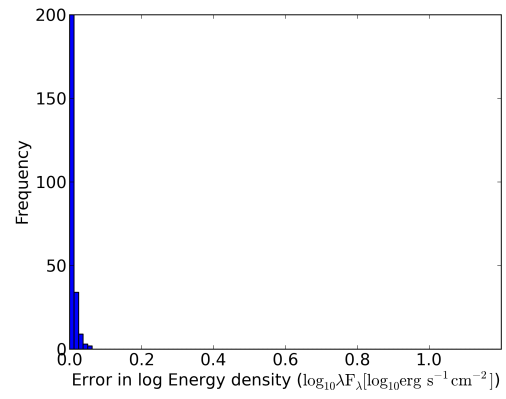
(a) F435W



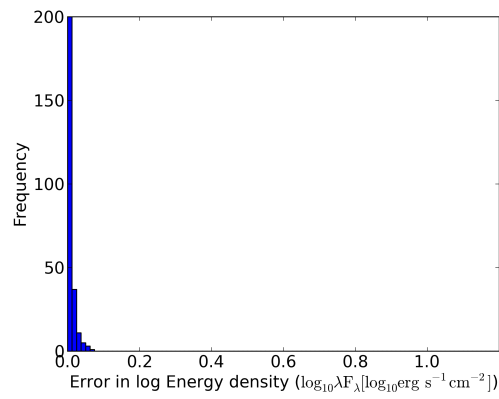
(b) F555W



(c) F658N



(d) F775W



(e) F850LP

Figure 14: Error in the flux of each filter.

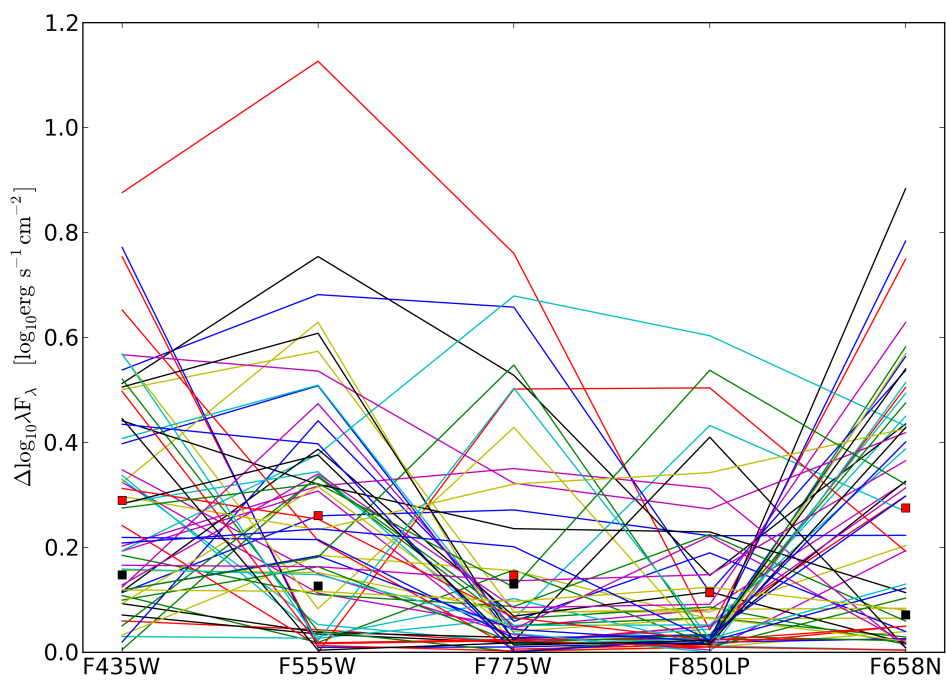


Figure 15: Variability of proplyds with an average variability over all ACS filters greater than the maximum photometric error in any of the filters. Each line is one proplyd. Red squares are the average variabilities in each filter of the depicted proplyds. Black squares are the average variabilities in each filter of the 201 proplyds with variability in any filter.

5 Analysis and Discussion

In order to assess the effects of the OB stars on proplyds in the Orion Nebula, the SEDs of the proplyds must be compared to those of YSOs in dark clouds. The central star of the proplyd and of the YSO should be of similar spectral type in order to reduce the effect of having different central stars. Through this comparison we want to assess how these environments affects planet formation and the evolution of the protoplanetary disk.

There are no SEDs published of the proplyds in Orion which contain photometry for the optical to submillimeter. However, Mann & Williams (2010) and Mann et al. (2014) have published SEDs for proplyds in the submillimeter to centimeter range. The shape of an SED is influenced by many variables. The main constituent parts of an SED can be seen in figures 16 and 17. The main difference in the SEDs of proplyds and those of these models is that these models do not take into account the cocoon around the star and disk in the proplyd. They only show the emission from the star and disk. The optical is dominated by the central star, and the longer wavelength regimes by the disk. In the infrared there three main features, a bump at $2\mu\text{m}$, a bump at $10\mu\text{m}$, and a wide peak at $30\text{-}100\mu\text{m}$. The bump at $2\mu\text{m}$ is due to emission by the inner rim of the disk (Dullemond et al. 2001), the bump at $10\mu\text{m}$ is due to silicates in the warm surface layers, and the far-infrared emission due to the outer disk regions. Emission in the submillimeter is due to the cold mid-plane of the outer disk regions. This emission can be used to estimate the disk mass of a proplyd (Mann & Williams 2010; Mann et al. 2014). Emission in $\text{H}\alpha$ is due to the presence of ionized gas in the ionization front of the proplyd. Other hydrogen recombination lines (Paschen and Balmer series) also contribute to the observed fluxes in the broad-band filters. Other atomic ionized species such as [NII], [OI], [OIII], and [SII] are also excited and emitted in the cocoon, and hence can contribute to the observed fluxes of broad-band filters. The effects of different disk geometries can be seen figure 18. These changes depend largely on the amount of incident flux on the different parts of the disk. Overall, the shapes of the SEDs are similar to those observed in regions such as Taurus. This tells us that the evolution of disks in the Orion Nebula is similar to that of disks in dark clouds.

There are many possible causes for the observed variabilities. These include shocks, jets, and outflows connected to the ongoing accretion of the disk onto the young star. The shocks caused by the accretion can excite and ionize material near the young star. This accretion of gas onto the young star also generates X-rays and UV, which inturn generate more flux from the disk.

One of the problems encountered in this work was finding an extinction for each proplyd. Proplyds which did not have an extinction were given the median extinction of objects in the Orion Nebula from Da Rio et al. (2012). In other cases the extinction catalogues gave an extinction of 0 for some objects. For objects with no extinction from any catalogue the extinction, or average extinction, of some nearby object within some radius could be used. This assumes that the extinction does not vary over short distances. However, the Orion Nebula is very

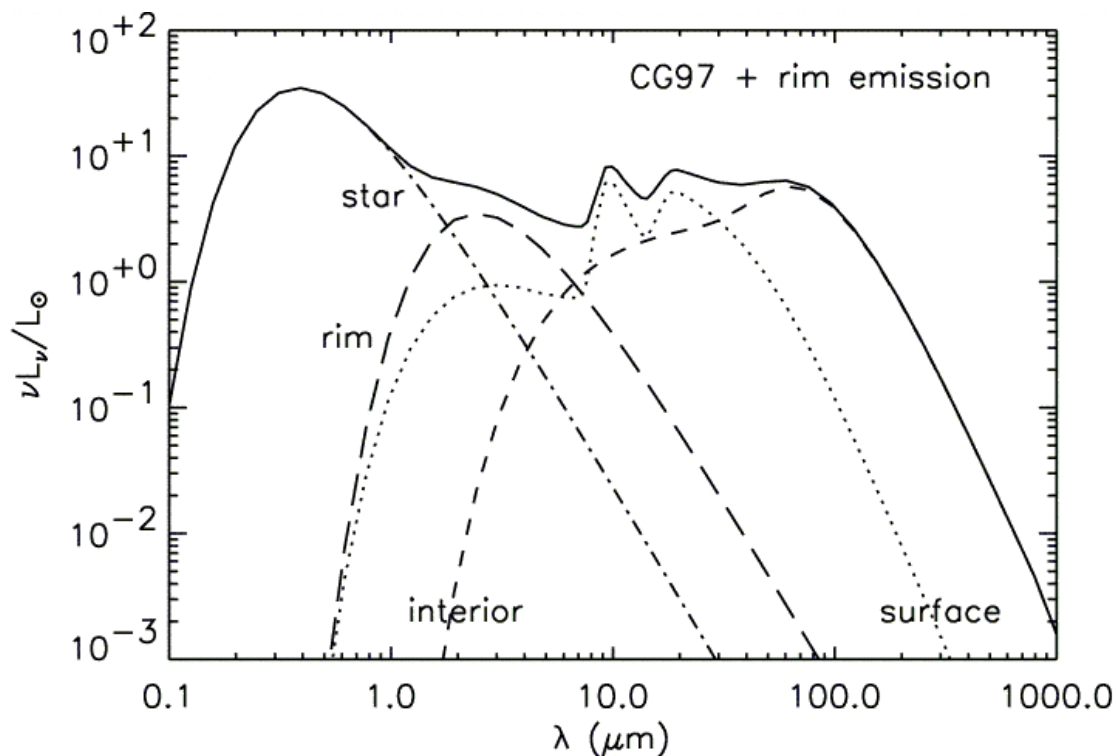


Figure 16: Model SED showing the sources of different features in an SED for a star and disk model. Figure is figure 4b in Dullemond et al. (2001).

patchy so this will introduce errors in the SED for objects which would use this method.

Some of the proplyds in the Orion Nebula are very near to other objects. This can cause the incorrect source to be used when searching for the photometry of the proplyds in the photometric catalogues. For example the photometry for 177-341E is contaminated by 177-341W. The near and mid-infrared photometric points are those of the much brighter 177-341W. A solution for this would be to check whether there are any nearby objects in the ACS source catalogue and compare their separation to the size of the aperture used when the photometry was done. If the separation is less than the aperture size the data point must be discarded.

For objects where both PSF and aperture photometry was available from Roberto et al. (2010) a comparison between them can be made. The PSF photometry shows the effect of the central star and the aperture photometry of the whole proplyd. For an object such as 072-135 in figure 7a it is clearly visible that the proplyd is brighter than the central star. On average for the J-, H-, and K-bands the ratios of the PSF fluxes to the aperture fluxes are 0.94, 0.96, 0.97, respectively.

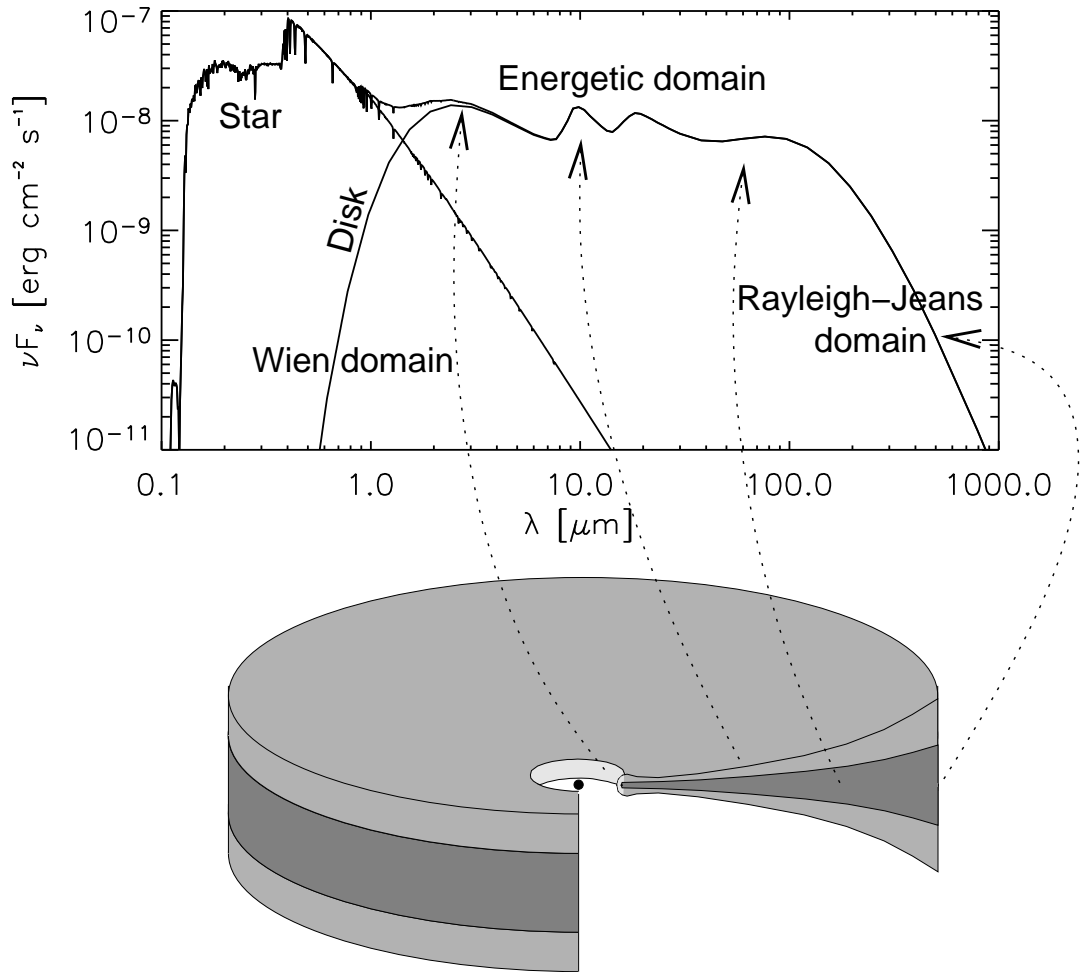


Figure 17: Build-up of the SED of a flaring protoplanetary disk and the origin of various components: the near-infrared bump comes from the inner rim, the infrared dust features from the warm surface layer, and the underlying continuum from the deeper (cooler) disk regions. Typically the near- and mid-infrared emission comes from small radii, while the far-infrared comes from the outer disk regions. The (sub-)millimeter emission mostly comes from the mid-plane of the outer disk. Scattering is not included here. Figure and caption from Dullemond et al. (2007).

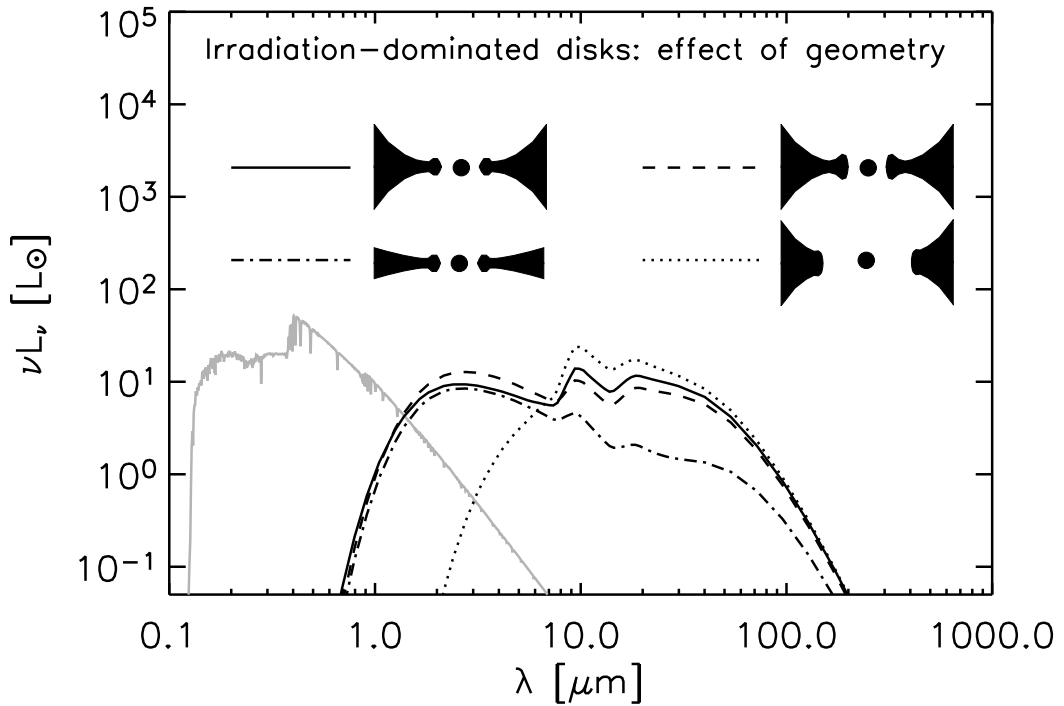


Figure 18: Overall SED shape for non-accreting disks with stellar irradiation. The stellar spectrum is added in grey-scale. Scattered light is not included in these SEDs. *Solid line* is normal flaring disk with inner dust rim; *dashed line* is when the rim is made higher; *dot-dashed line* is when the flaring is reduced (or when the disk becomes ‘self-shadowed’); *dotted line* is when the inner rim is at 10 times larger radius. Figure and caption from Dullemond et al. (2007).

6 Conclusion

This work has a lot of opportunity for expansion. The main issue with these SEDs is the empty region ranging from around $50 \mu\text{m}$ to $800 \mu\text{m}$. The lack of photometry here makes it difficult to distinguish the disk properties. Observations by ALMA could reduce the span of this gap to $50 - 300 \mu\text{m}$. It is difficult to cover the remaining far infrared gap as the Orion Nebula is very bright in this regime, and so the signal would be very difficult to detect over the background. In order to detect and distinguish the proplyds from the high nebular emission the required telescope would need to have a very high spatial resolution and a high sensitivity. The Earth's atmosphere strongly absorbs the radiation in this regime. This requires that the telescope be in space or above a significant portion of the atmosphere. Telescopes with the ability to see in this regime are the *Herschel Space Telescope*, the *Spitzer Space Telescope*, and *Stratospheric Observatory for Infrared Astronomy (SOFIA)*. However, the spatial resolution of these telescopes is too low to effectively image the proplyds in this work.

The immediate follow-up of this work is to include observations in the X-ray regime. X-rays can assist in finding the age of proplyds. They also indicate whether accretion is occurring. X-rays generated by this accretion, as well as the $\text{H}\alpha$ flux densities, and the variability of the proplyd could give a good insight of the accretion rate. The X-rays can also heat and ionize the gas in the surface regions of the disks. This additional heating will then be visible in the near infrared. Having the X-rays included in the SEDs may give an insight into this effect and probe the properties of the central star.

With these SEDs it is possible to create a typical SED for proplyds of the same type. This allows for typical features common to each type of proplyds to be deduced. An other possible use would be in cases where the proplyd cannot be resolved. The proplyd type can then be deduced by comparing it to the different typical SEDs. This can be expanded on by creating typical SEDs of proplyds at different distances from the Trapezium.

Finally, models can be fit to the SEDs. This allows for estimates to be made of the properties of the proplyds, such as the stellar mass, stellar temperature, the inner radius of the disk, viewing angle, and more (Robitaille et al. 2006).

7 Acknowledgments

I would like to thank my supervisor Silvia Vicente for her guidance and advice. I would also like to thank Pablo Rivière for our useful discussions. Finally, I would like to thank Inga Kamp for her insightful comments and encouragement.

8 Bibliography

- Boss, A. P., Ipatov, S. I., Keiser, S. A., Myhill, E. A., & Vanhala, H. A. T. 2008, *Astrophysical Journal, Letters*, 686, L119
- Cardelli, J. A., Clayton, G. C., & Mathis, J. S. 1989, *Astrophysical Journal*, 345, 245
- Costero, R. & Peimbert, M. 1970, *Boletín de los Observatorios Tonantzintla y Tacubaya*, 5, 229
- Cutri, R. M. & et al. 2012, *VizieR Online Data Catalog*, 2311, 0
- Da Rio, N., Robberto, M., Hillenbrand, L. A., Henning, T., & Stassun, K. G. 2012, *Astrophysical Journal*, 748, 14
- Da Rio, N., Robberto, M., Soderblom, D. R., et al. 2009, *Astrophysical Journal, Supplement*, 183, 261
- Da Rio, N., Robberto, M., Soderblom, D. R., et al. 2010, *Astrophysical Journal*, 722, 1092
- Dullemond, C. P., Dominik, C., & Natta, A. 2001, *Astrophysical Journal*, 560, 957
- Dullemond, C. P., Hollenbach, D., Kamp, I., & D'Alessio, P. 2007, *Protostars and Planets V*, 555
- Feigelson, E. D., Broos, P., Gaffney, III, J. A., et al. 2002, *Astrophysical Journal*, 574, 258
- Garay, G., Moran, J. M., & Reid, M. J. 1987, *Astrophysical Journal*, 314, 535
- Getman, K. V., Feigelson, E. D., Grosso, N., et al. 2005a, *Astrophysical Journal, Supplement*, 160, 353
- Getman, K. V., Flaccomio, E., Broos, P. S., et al. 2005b, *Astrophysical Journal, Supplement*, 160, 319
- Hillenbrand, L. A. 1997, *Astronomical Journal*, 113, 1733
- Hillenbrand, L. A. & Carpenter, J. M. 2000, *Astrophysical Journal*, 540, 236
- Hillenbrand, L. A., Hoffer, A. S., & Herczeg, G. J. 2013, *Astronomical Journal*, 146, 85

- Hillenbrand, L. A., Strom, S. E., Calvet, N., et al. 1998, *Astronomical Journal*, 116, 1816
- Johnstone, D., Hollenbach, D., & Bally, J. 1998, *Astrophysical Journal*, 499, 758
- Kraus, S., Weigelt, G., Balega, Y. Y., et al. 2009, *Astronomy and Astrophysics*, 497, 195
- Kryukova, E., Megeath, S. T., Gutermuth, R. A., et al. 2012, *Astronomical Journal*, 144, 31
- Lada, C. J., Muench, A. A., Lada, E. A., & Alves, J. F. 2004, *Astronomical Journal*, 128, 1254
- Laques, P. & Vidal, J. L. 1979, *Astronomy and Astrophysics*, 73, 97
- Lucas, P. W., Roche, P. F., & Tamura, M. 2005, *Monthly Notices of the RAS*, 361, 211
- Luu, J. X. & Jewitt, D. C. 2002, *Annual Review of Astron and Astrophys*, 40, 63
- Mann, R. K., Di Francesco, J., Johnstone, D., et al. 2014, *Astrophysical Journal*, 784, 82
- Mann, R. K. & Williams, J. P. 2010, *Astrophysical Journal*, 725, 430
- Menten, K. M., Reid, M. J., Forbrich, J., & Brunthaler, A. 2007, *Astronomy and Astrophysics*, 474, 515
- Muench, A. A., Lada, E. A., Lada, C. J., & Alves, J. 2002, *Astrophysical Journal*, 573, 366
- O'Dell, C. R., Wen, Z., & Hu, X. 1993, *Astrophysical Journal*, 410, 696
- Renson, P. & Manfroid, J. 2009, *Astronomy and Astrophysics*, 498, 961
- Ricci, L., Robberto, M., & Soderblom, D. R. 2008, *Astronomical Journal*, 136, 2136
- Richling, S. & Yorke, H. W. 2000, *Astrophysical Journal*, 539, 258
- Robberto, M., Beckwith, S. V. W., Panagia, N., et al. 2005, *Astronomical Journal*, 129, 1534
- Robberto, M., Soderblom, D. R., Bergeron, E., et al. 2013, *The Astrophysical Journal Supplement Series*, 207, 10
- Robberto, M., Soderblom, D. R., Scandariato, G., et al. 2010, *Astronomical Journal*, 139, 950
- Robitaille, T. P., Whitney, B. A., Indebetouw, R., Wood, K., & Denzmore, P. 2006, *Astrophysical Journal, Supplement*, 167, 256

Smith, N., Bally, J., Shuping, R. Y., Morris, M., & Kassis, M. 2005, *Astronomical Journal*, 130, 1763

Störzer, H. & Hollenbach, D. 1999, *Astrophysical Journal*, 515, 669

Vicente, S., Berné, O., Tielens, A. G. G. M., et al. 2013, *Astrophysical Journal Letters*, 765, L38

Vicente, S. M. & Alves, J. 2005, *Astronomy and Astrophysics*, 441, 195